DOT/FAA/TC-16/35

Federal Aviation Administration
William J. Hughes Technical Center
Aviation Research Division
Atlantic City International Airport
New Jersey 08405

Certification of Discontinuous Fiber Composite Structures via Stochastic Modeling

May 2017

Final Report

U.S. Department of Transportation
Federal Aviation Administration

NOTICE

Technical Report Documentation Page

1. Report No.	2. Government Accession No.	3. Recipient's Catalog No.
DOT/FAA/TC-16/35		

4. Title and Subtitle	5. Report Date
CERTIFICATION OF DISCONTINUOUS FIBER COMPOSITES VIA STOCHASTIC MODELING	May 2017
	6. Performing Organization Code

7. Author(s)	8. Performing Organization Report No.
Karen Harban and Mark Tuttle	

9. Performing Organization Name and Address	10. Work Unit No. (TRAIS)
Department of Mechanical Engineering, MS 352600 University of Washington Seattle, WA 98195-2600	11. Contract or Grant No.

12. Sponsoring Agency Name and Address	13. Type of Report and Period Covered
FAA Northwest Mountain Regional Office 1601 Lind Ave SW Renton, WA 98057	14. Sponsoring Agency Code AIR 100

15. Supplementary Notes

The Federal Aviation Administration William J. Hughes Technical Center Aviation Research Division CORs were Lynn Pham and Curtis Davies.

16. Abstract

The overall goal of this study is to assess a numerical modeling approach that will ultimately lead to a cost-effective certification process for discontinuous fiber composite (DFC) structures based on analysis and supported by modest experimental verification. A commercially-available DFC material system known as HexMC™ was used as a model DFC during the study. The stochastic laminate analogy (SLA), a stochastic (Monte Carlo-type) finite element modeling approach, was developed and used to predict the stiffness and strength of HexMC tensile specimens. Experimentally observed variations in the tensile stiffness and notched and unnotched fracture strength of HexMC are then simulated by performing many finite element analyses, in which new random stacking sequences are generated during each analysis. Fracture predictions were obtained through a damage accumulation model based on the ply discount scheme. A typical analysis predicts that ply failures (i.e., "damage") evolve in a distributed manner throughout the HexMC specimen, even in the presence of stress risers. This damage pattern is in qualitative agreement with experimental observation. B-basis, Bmax, and average measures of modulus and fracture strengths are predicted using the SLA modeling approach.

It is predicted that relatively thin HexMC specimens (e.g., less than approximately 16–18 chips thick, or 0.08 to 0.09 inch) will exhibit relatively low average tensile stiffness with a high level of variation. As thickness is increased, average tensile stiffness converges to a near-constant value, and the coefficient of variation (CoV) decreases. The average tensile stiffness of thick HexMC specimens is predicted to be approximately 92% of the corresponding quasi-isotropic value, with a CoV of approximately 18%.

Fracture predictions were hampered by the extreme computational expense associated with the SLA approach. However, the expense can be reduced by developing a specialized software package that implements on the recommendations presented herein. In addition, failure predictions were based on a failure criterion (i.e., the Tsai-Wu criterion) that cannot capture important failure modes such as delamination. Nevertheless, the SLA approach was able to predict important experimental observations. For example, the analysis showed that fractures of open-hole tensile specimens with a *d/w* ratio of less than approximately 0.083 will normally occur away from the hole, rather than at the hole. As the hole size is increased (i.e., as the *d/w* ratio is increased) the likelihood of fracture at the hole is increased. For *d/w* greater than 0.33, most fractures will occur at the hole.

The SLA approach shows great promise in predicting the elastic and fracture behavior of DFC structures. Once perfected, the SLA approach may lead to an enormous decrease in certification costs of DFC structures. The primary areas of improvement needed are an improved chip failure model and a substantial reduction in computation times.

17. Key Words	18. Distribution Statement
Discontinuous fiber composite, Stochastic laminate analogy	This document is available to the U.S. public through the National Technical Information Service (NTIS), Springfield, Virginia 22161. This document is also available from the Federal Aviation Administration William J. Hughes Technical Center at actlibrary.tc.faa.gov.

19. Security Classif. (of this report)	20. Security Classif. (of this page)	21. No. of Pages	22. Price
Unclassified	Unclassified	58	

ACKNOWLEDGEMENTS

The authors gratefully acknowledge the financial and technical support provided throughout this study by Dr. Larry Ilcewicz and Mr. Curtis Davies of the FAA; Dr. William Avery of the Boeing Company; and Mr. Bruno Boursier and Mr. David Barr of the Hexcel Corporation. The authors also gratefully acknowledge former graduate students at the University of Washington who contributed to this study, including Mr. Tory Shifman (MSME ’11), Mr. Brian Head (MSME ’13), and Mr. Michael Arce (MSME ’15).

TABLE OF CONTENTS

LIST OF FIGURES

LIST OF TABLES

LIST OF ACRONYMS

B787	Boeing 787
BMC	Bulk molding compound
CAD	Computer-aided design
CLT	Classical lamination theory
CoV	Coefficient of variation
DFC	Discontinuous fiber composite
FEM	Finite element model
GPa	Gigapascal
MNR	Maximum normal residual
RLVE	Random laminate volume element
SLA	Stochastic laminate analogy
SMC	Sheet molding compound
UW	University of Washington

EXECUTIVE SUMMARY

The overall goal of this study is to assess a numerical modeling approach that will ultimately lead to a cost-effective certification process for discontinuous fiber composite (DFC) structures based on analysis and supported by modest experimental verification. A commercially available DFC material system known as HexMC™ was used as a model DFC during the study. The stochastic laminate analogy (SLA), a stochastic (Monte Carlo-type) finite element modeling approach, was developed and used to predict the stiffness and strength of HexMC tensile specimens. During a typical analysis, the HexMC specimen is divided into regions called random laminate volume elements (RLVEs). A unique randomly generated and non-symmetric stacking sequence is assigned to each RLVE. Stacking sequences in neighboring RLVEs are therefore completely independent. Experimentally observed variations in the tensile stiffness and notched and unnotched fracture strength of HexMC are then simulated by performing many finite-element analyses, in which a new random stacking sequence is generated for all RLVEs during each analysis. Fracture predictions were obtained through a damage accumulation model based on the ply discount scheme. A typical analysis predicts that ply failures (i.e., "damage") evolve in a distributed manner throughout the HexMC specimen, even in the presence of stress risers. This damage pattern is in qualitative agreement with experimental observations. In this study, the SLA modeling approach is used to predict B-basis, Bmax, and average elastic modulus and B-basis and average tensile strength.

It is predicted that relatively thin HexMC specimens (e.g., less than approximately 16–18 chips thick) will exhibit relatively low average tensile stiffness with a high level of variation. Average tensile stiffness converges to a near-constant value, and the coefficient of variation (CoV) decreases as thickness is increased (for thicknesses greater than approximately 18 chips). The average tensile stiffness of thick HexMC specimens is predicted to be approximately 92% of the corresponding quasi-isotropic value, with a CoV of approximately 18%.

Fracture predictions were hampered by the extreme computational expense associated with the SLA approach. The computational expense encountered during this study was due to handshaking between several general-purpose software packages (e.g., handshaking between a Visual Basic program written in-house, FEMAP, NX Nastran, and Excel). In future studies this expense can be eliminated by developing a standalone software package that implements the SLA approach. In addition, failure predictions were based on a failure criterion (i.e., the Tsai-Wu criterion) that cannot capture important failure modes, most notably delamination failures between chips. Nevertheless, the SLA approach was able to predict important experimental observations. For example, the analysis showed that fractures of open-hole tensile specimens with a *d/w* ratio of less than approximately 0.083 will normally occur away from the hole, rather than at the hole. As the hole size is increased (i.e., as the *d/w* ratio is increased), the likelihood of fracture at the hole is increased. For *d/w* greater than 0.33, most fractures will occur at the hole.

The SLA approach shows great promise in predicting the elastic and fracture behavior of DFC structures. Once perfected, the SLA approach may lead to an enormous decrease in certification costs of DFC aircraft structures. The primary areas of improvement needed are an improved ply failure model (used to predict the evolution of distributed damage and final fracture) and development of a standalone software package that implements SLA approach.

1. INTRODUCTION

Polymeric composite materials are being used to an ever-increasing extent in commercial transport aircraft because of the high strength-to-weight and stiffness-to-weight ratios these materials exhibit. Examples of recent aircraft that use polymeric composite materials include The Boeing Company 787 (B787) Dreamliner and the Airbus A350, both of which use approximately 50% composites by weight [1, 2].

Both continuous-fiber composites and discontinuous fiber composites (DFCs) are used in the B787 and A350. Continuous-fiber composites are based on very long fibers (i.e., fibers that are long enough to be considered "continuous"). Continuous-fiber composites are most commonly used to produce multi-ply (laminated) structures, in which fiber angles vary from one ply to the next. The number of plies and ply fiber angles, collectively known as the "stacking sequence" of the laminate, can be selected to achieve required directional strength and stiffness.

In contrast, relatively short fibers are used in DFC material systems. DFCs are often grouped into two broad categories: bulk molding compounds (BMCs) and sheet molding compounds (SMCs) [3]. In most industries, BMCs and SMCs usually consist of randomly oriented glass fibers embedded within a polyester matrix, though other forms are commercially available[1]. BMCs are based on fiber lengths ranging from approximately 0.8–12 mm (0.03–0.5 in), and BMC parts are usually produced using injection molding. In contrast, SMCs are based on fiber lengths ranging from approximately 12–100 mm (0.5–4 in), and SMC parts are usually produced using compression molding. Because of their longer fiber lengths, SMCs exhibit higher stiffness and strengths than BMCs. Both BMCs and SMCs have been commercially available for decades and are widely used to produce, for example, household goods and automotive parts.

For a given fiber/matrix combination, continuous-fiber composites exhibit higher stiffness- and strength-to-weight ratios than comparable DFCs. Consequently, in the past, DFCs have not been used in critical load-bearing parts in transport aircraft. However, a new generation of DFCs has emerged and is being used in load-bearing applications in both the B787 and A350 aircraft. Specifically, a DFC called HexMC™ is used in both of these aircraft [4, 5].

HexMC is produced using chipped B-staged AS4/8552R graphite epoxy unidirectional prepreg, as shown in figure 1. First, a unidirectional ply of AS4/8552R is slit, chopped, and randomly deposited on a release backing, forming a layer of HexMC prepreg (see figure 1(a)). Nominal chip dimensions are 0.127 mm x 7.6 mm x 50 mm (0.005 in x 0.30 in x 2 in). The number of through-thickness chips varies spatially because of the random nature of the deposition process, but typically approximately eight through-thickness chips exist at any point in the layer. The prepreg layer is placed on a roll (see figure 1(b)) and stored in a freezer until needed.

[1] For example, bulk and sheet molding compounds based on carbon fibers embedded in vinyl ester or epoxy resins are available.

(a) (b)

Figure 1. Producing a roll of HexMC prepreg: (a) chips of B-staged unidirectional AS4/8552R graphite-epoxy chips being randomly deposited on a release backing, and (b) HexMC prepreg being rolled up for freezer storage until needed

Compression molding of a prototype HexMC window frame is shown in figure 2. First, HexMC pieces are cut in specified shapes from a parent roll of prepreg. The HexMC pieces are placed by hand into a preheated matched-metal mold. The mold is closed and heat and pressure are applied, causing the HexMC part to consolidate and cure. The part is removed from the mold once cure is complete, resulting in a near-net shape part.

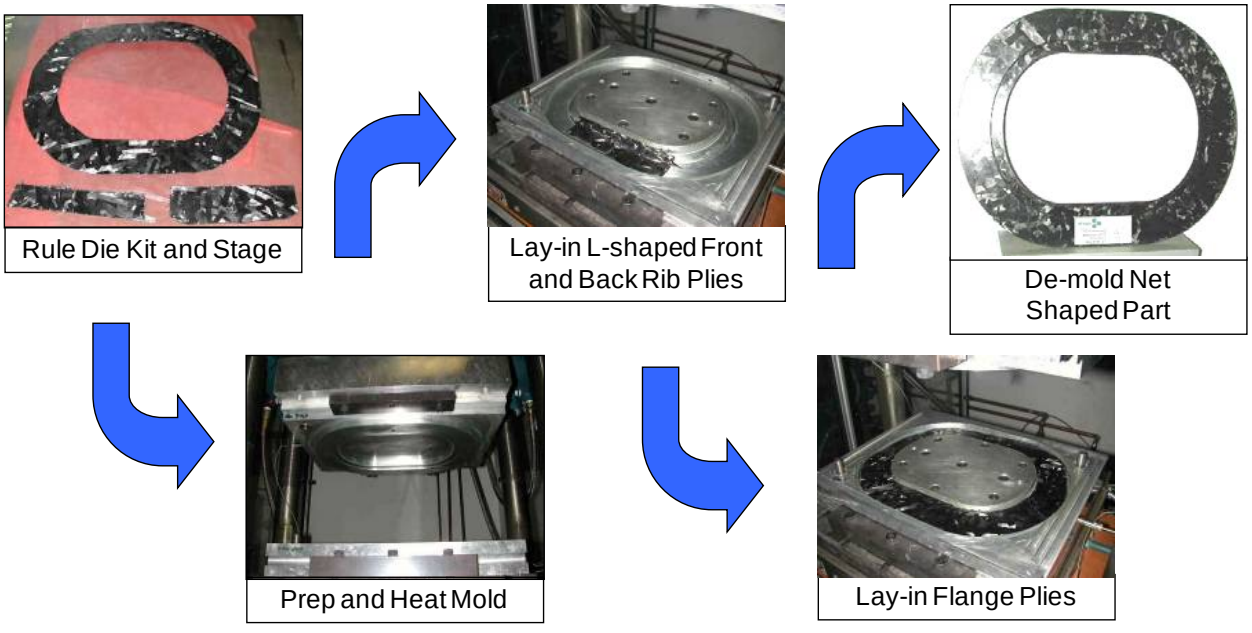

Figure 2. Compression molding of a prototype window frame using HexMC

The randomly oriented chips can be readily seen on an external surface of a HexMC part, as shown in figure 3(a). Micrographs of typical through-thickness chip structure are presented in figures 3(b) and (c). Together these images show that HexMC parts can be approximately

visualized as a laminated composite part in which the local stacking sequence (as represented by the local through-thickness chip structure) varies continuously throughout the part.

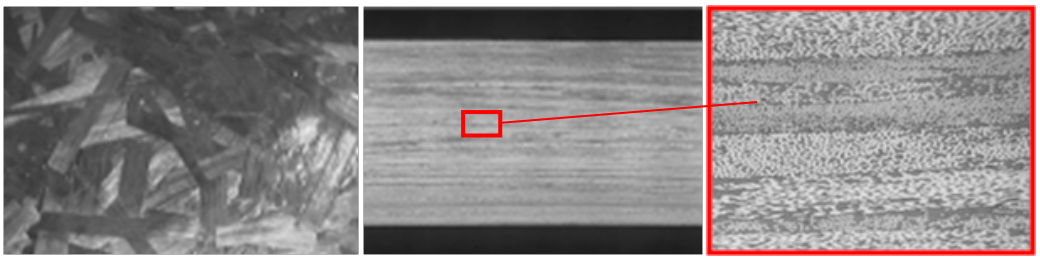

(a) (b) (c)

Figure 3. Images illustrating the chip structure of a cured HexMC part: (a) the typical surface of a HexMC part, showing random orientation of AS4/8552 chips, (b) the edge view of a HexMC part, and (c) the magnified edge view of a HexMC part, showing approximately laminar through-thickness chip structure

1.1 PROBLEM STATEMENT

HexMC is being used in load-bearing parts within the B787 and A350 aircraft because it is relatively easy to manufacture compression-molded HexMC parts with complex shapes and because HexMC exhibits near quasi-isotropic in-plane stiffness and strengths [6] and high delamination resistance. Though HexMC provides many advantages, there are also significant disadvantages. In particular, HexMC exhibits high levels of scatter in stiffness and strength properties and notch insensitivity, compared with continuous-fiber composites [6, 7]. Consequently, it is difficult to perform rigorous structural analyses of HexMC parts with a high level of confidence. Because rigorous analytical predictions are difficult, certification of HexMC parts within the B787 and A350 aircraft were achieved through extensive experimental testing. This is a time consuming and costly approach and probably leads to over-conservative part designs. Analytical/numerical methods capable of accurately predicting the statistical variation of stiffness and strength of DFC parts are greatly needed by the aircraft industry. If suitable and cost-effective analysis procedures are developed, then a new, far less costly certification process based on analysis supplemented by relatively modest experimental measurements will emerge.

1.2 OBJECTIVES

The overall goal of this study is to help establish methods to certify prepreg-based DFC aircraft parts. Towards that end, a previously developed stochastic finite element modeling approach called the stochastic laminate analogy (SLA) [8, 9] was applied to the HexMC material system during this study. Specific tasks were:

1. Use the SLA to predict B-basis and Bmax tensile moduli for simple HexMC tensile coupon specimens.
2. Develop a practical failure criterion coupled with the SLA and suitable for use with HexMC structures.
3. Predict the B-basis tensile strengths for unnotched and notched HexMC tensile coupons.

2. BACKGROUND REVIEW

2.1 THE STOCHASTIC LAMINATE ANALOGY

Halpin and colleagues were among the first to study the mechanical behavior of DFCs. Their studies showed that DFCs could be treated (mathematically) as laminated composite systems. The analysis techniques developed during these studies are now known collectively as the "Laminate Analogy." That is, it was shown that under proper circumstances, various analysis methods developed for use with laminated continuous-fiber composites may also be applied to DFCs. Initial efforts focused on thin plate-like structures, about which it can be assumed that the average length of the short fibers is larger than the plate thickness. It was shown that in-plane stiffness of quasi-isotropic [0/90/±45] laminates consisting of layers of oriented short fibers of known volume fraction v_f and aspect ratio l/d were equal to those exhibited by a sheet of randomly oriented short fibers of equivalent v_f and l/d [10]. Tensile strengths of randomly orientated short-fiber composites were also successfully predicted using the maximum strain failure criterion and a ply-discount scheme [11].

Conversely, manufacturing processes used to produce DFC parts may result in through-thickness variations of fiber orientation (this is particularly true of injection-molded or extruded parts). In these cases, fiber orientations are not random and in-plane stiffness and strength will not be quasi-isotropic. In these cases, the DFC can be treated as a laminate consisting of a stack of unidirectional plies, of which the volume fraction and orientation of each ply reflects the percentage of discontinuous fibers at each orientation in the actual material [12].

In 2010, Feraboli and his colleagues applied a modified version of the laminate analogy to the study of prepreg-based DFCs such as HexMC [13]. Their approach involves performing multiple analyses with randomly selected fiber angles, known as the SLA. In this approach, a HexMC structure is modeled by defining discrete regions called random laminate volume elements (RLVEs) within the overall structure. Each RLVE is treated as a continuous-fiber laminate, in which the number of plies within the laminate equals the number of through-thickness chips in the actual HexMC part. The fiber angles for each RLVE are selected randomly, reflecting the random chip orientations within a HexMC part. A shortcoming of the SLA originally presented by Feraboli et al. [13] was that symmetric stacking sequences were assumed for the RLVEs even though fiber orientations were selected randomly. This removes potential membrane-bending coupling effects that may occur and, therefore, does not reflect the random non-symmetric chip orientations within a HexMC part. This restriction was later removed by Head and Tuttle [8, 14] by randomly selecting all plies/chip orientations within an RLVE; symmetry is no longer enforced. After defining all regions of a structure of interest in terms of RLVEs with random stacking sequences, the structure is then discretized using standard finite-element processes. The stacking sequence of an individual element corresponds to the RLVE in which the element resides.

The entire analysis process is repeated many times, and new random stacking sequences are generated for all RLVEs during each analysis. The repeated analyses of the HexMC structure with random stacking sequences is intended to capture the variable stiffness and strengths exhibited by HexMC structures.

An appropriate RLVE size must be established to apply the SLA approach. Feraboli et al [13] used an RLVE size of approximately 12.7 mm x 12.7 mm (0.5 inch x 0.5 inch). Later, Head [8] performed a detailed numerical study based on FE analyses using different RLVE sizes. He compared the predicted variation in surface strains with experimental measurements obtained using Digital Image Correlation. He concluded that the optimal RLVE size was approximately 19.1mm x 19.1 mm (0.75 in x 0.75 in). Head also performed a mesh sensitivity study [8]. He found that predicted in-plane strain variations, particularly near the boundaries between RLVEs, were best predicted using elements with nominal dimension of 3.18 mm (0.125 inch).

The conclusions from the Head analyses were implemented during this study. That is, wherever possible, square RLVEs were used with dimensions of 19.1mm x 19.1 mm (0.75 in x 0.75 in), and the RLVEs themselves were described using nominally square finite elements with dimensions of 3.18 mm x 3.18 mm (0.125 in x 0.125 in). This implies that, wherever possible, 36 elements were used within each RLVE. In some cases, it is not possible to use strictly square RLVEs or square finite elements. For example, when modeling an open-hole tensile specimen, non-square RLVE regions and non-square finite elements are inevitable. In these cases, nominal RLVE sizes and finite-element dimensions were maintained as close to 19.1 mm and 3.18 mm (respectively) as possible. It is worth noting that the appropriate RLVE size and mesh density for use in modeling DFC structures is likely related to chip size. The RLVE size and finite element dimensions used during this study are recommended for when modeling HexMC, which has chip dimensions of approximately 0.127 mm x 7.6 mm x 50 mm (0.005 in x 0.30 in x 2 in). These RLVE and finite element sizes may not be appropriate when modeling a DFC with a substantially different chip size, however.

In this study, the SLA was used to predict the stiffness and strength of HexMC tensile specimens. Numerical computer-aided design (CAD) models of the tensile specimens were first generated using SOLIDWORKS[2]. The CAD models were then imported to Femap™ software and prepared for analysis using the NX Nastran™ software finite-element solver[3]. Laminated shell elements with 2-D orthotropic properties were used in all cases. Predictions of HexMC tensile stiffness using the SLA are discussed in section 3, and predictions of tensile strengths are discussed in section 4.

2.2 HEXMC MATERIAL PROPERTIES

Two grades of HexMC are produced by the Hexcel Corporation. One is called “industrial grade HexMC,” and the second is called “aerospace grade HexMC”. Mechanical properties of industrial-grade HexMC laminates are available [15]. Properties of aerospace-grade HexMC laminates are proprietary, but are thought to be similar to industrial-grade HexMC.

The SLA requires that calculations be performed at the ply level (or, in the context of HexMC, at the chip level). Chip properties are not available for either industrial- or aerospace-grade HexMC. Because HexMC is produced using unidirectional AS4/8552R prepreg, during this

[2] SOLIDWORKS is a CAD software package produced by Dassault Systèmes (http://www.solidworks.com/)
[3] Femap and NX Nastran are available from Siemens PLM Software (http://www.plm.automation.siemens.com/en_us/products/femap/)

study it was assumed that HexMC chip properties can be equated to properties of the unidirectional AS4/8552 material system. However, differing values for elastic and strength properties of unidirectional AS4/8552 have appeared in the literature. For example, the fiber-dominated modulus E11 for AS4/8552 is reported to be 132 GPa (19.1 Msi) by Marlett [16], whereas McGowan and Ambur [17] report a value of 112 GPa (16.3 Msi), a difference of 17%. A further complication is that significantly different average values of HexMC properties have also been reported. For example, the average tensile stiffness of HexMC has been reported to be 43.2 GPa [6], 45.6 GPa [7], 41.2 GPa [13], and 38 GPa [15], a range of 20%. During this study, it was ultimately decided to assume values of elastic and strength properties for AS4/8552 that lead to quasi-isotropic stiffness and strengths similar to those reported by Feraboli [7]. The stiffness and strength properties assumed for HexMC chips are presented in tables 1 and 2. The thickness of a single chip was assumed to be 0.127 mm (0.005 in).

Table 1. Elastic properties assumed for unidirectional HexMC chips

E_{11}	E_{22}	G_{12}	ν_{12}
118 GPa (17.1 Msi)	8.0 GPa (1.16 Msi)	4.45 GPa (0.646 Msi)	0.32

Table 2. Strength properties assumed for unidirectional HexMC chips

0° Strength		90° Strength		In-plane Shear Strength
Tensile	Compression	Tensile	Compression	
1010 MPa (147 ksi)	950 MPa (138 ksi)	37.0 MPa (5.38 ksi)	47.5 MPa (6.89 ksi)	52.6 MPa (7.63ksi)

2.3 CALCULATING DESIGN ALLOWABLES

Numerical values of material properties used during the design of an aircraft structure are based on a statistical analysis of a suitable database. Two statistical measures are commonly defined: A-basis design allowables and B-basis design allowables. A- and B-basis strengths are probably most commonly encountered, though the statistical definition can be applied to any property of interest. For example, it is possible to define a B-basis modulus, density, thermal conductivity, diffusivity, etc.

B-basis (and A-basis) values are defined as the value that 90% (or 99% for A-basis) of the measured values will exceed, with a 95% confidence level. Only B-basis properties were considered during this study, so A-basis properties will not be further discussed. During this study, B-Basis properties were calculated based on both: (1) numerical predictions obtained using the SLA, and (2) proprietary measurements provided by Hexcel[4].

[4] Only normalized values of proprietary data are presented herein.

An additional measure of B-basis stiffness was defined during this study. The measured values of the elastic modulus of HexMC exhibit a higher scatter than is typical of other composite material systems [6]. That is, the elastic modulus may vary significantly over differing regions within a HexMC structure. At various points the stiffness may be significantly lower or significantly higher than the average value. In general, the traditional B-basis stiffness can be interpreted as the lowest stiffness value that HexMC is likely to exhibit. A second design-allowable value for stiffness was defined during this study: the Bmax stiffness value. The Bmax stiffness was defined as the value that exceeds 90% of the measured values, with a 95% confidence level. In general, the Bmax stiffness can be interpreted as the highest stiffness value that HexMC is likely to exhibit.

All B-basis calculations followed the guidelines described by Tomblin et al. [18]. For convenience, calculation steps for B-basis values are summarized in this section. Refer to the Tomblin et al. [18]/Shyprykevich [19] for a broader discussion of the statistical underpinnings of B-basis calculations.

The general procedure to compute B-basis allowables from a composites database begins with: (1) normalizing the raw test data by volume fraction and (2) grouping data by test environment. This step was not required in this study because neither volume fraction nor multiple test environments were considered.

The sample mean, $\bar{x}$, and standard deviation, s, are calculated, based on the number of available observations, n:

$$\bar{x} = \frac{1}{n}\sum_{i=1}^{n} x_1 \tag{1}$$

$$s^2 = \frac{1}{n-1}\sum_{i=1}^{n}\left(x_i - \bar{x}\right)^2 \tag{2}$$

The next step is to check if there are outliers present in the data. Methods used to check for outliers may be a simple visual representation of graphical plots of the data, or a quantitative numerical procedure. The maximum normal residual (MNR) method is the most commonly used numerical procedure [18]. According to the MNR test, a particular measurement is judged to be an outlier if the absolute value of the difference between the measurement and the sample mean is too large to be due to chance. The MNR statistic is calculated as follows:

$$MNR = \max_i \frac{\left|x_i - \bar{x}\right|}{s}, i = 1,2,...,n \tag{3}$$

The MNR statistic is compared to the critical value of the so-called *t*-distribution with *n*-2 degrees of freedom. Critical values for *n* ranging from 3–200 are tabulated in Tomblin et al. [18]. If the MNR statistic is greater than the critical value, then the corresponding measurement is judged to be an outlier. If an outlier exists, then a series of steps are taken to decide whether the measurement should be retained or deleted from the database [18]. If an outlier is removed, then

a revised sample mean, $\bar{x}$, and standard deviation, s, are calculated, and the *MNR* test repeated until all outliers have been accounted for.

The next step is to determine whether the data is well-approximated by an assumed distribution function. In this study, the data was assumed to follow a normal (i.e., Gaussian) distribution. Measurements were divided by the mean value and arranged in ascending order. The probability of survival at each value was then computed using equation (4):

$$\text{Probability of survival at } x_i = 1 - \frac{i}{n+1} \tag{4}$$

Calculated values are compared to the (assumed) normal distribution. Engineering judgment is used to assess whether measurements follow the assumed distribution.

Next, the B-basis tolerance factor k_b is estimated by:

$$k_b = z_b\sqrt{\frac{f}{Q}} + \sqrt{\frac{1}{n*C_B} + \left(\frac{b_B}{2C_B}\right)^2} - \frac{b_B}{2C_B} \tag{5}$$

where $f = n–2$ represents the degrees of freedom variance. Variables z_b, b_B, and C_B all take on values dictated by B-basis calculations (i.e., values appropriate for 90% probability) and by f (i.e., by the number of observations n, because $f = n–2$). For a normal distribution and 90% probability, $z_b = 1.28115$. Coefficients b_B and C_B are given by:

$$b_B = 1.1372\frac{1}{\sqrt{f}} - 0.49162\frac{1}{f} + 0.18612\frac{1}{f\sqrt{f}} \tag{6}$$

$$C_B = 0.36961 + 0.0040342\frac{1}{\sqrt{f}} - 0.71750\frac{1}{f} + 0.19693\frac{1}{f\sqrt{f}} \tag{7}$$

Variable Q is strictly a function of f and is given by:

$$Q = f - 2.327\sqrt{f} + 1.138 + 0.6057\frac{1}{\sqrt{f}} - 0.3287\frac{1}{f} \tag{8}$$

Finally, the B-basis value is given by:

$$B_{basis} = \bar{x} - (k_b)s \tag{9}$$

During this study, equation (9) was used to calculate both B-basis stiffness and B-basis strength values. The Bmax stiffness was also defined and calculated as follows:

$$B_{\max} = \bar{x} + (k_b)s \tag{10}$$

3. PREDICTED HEXMC TENSILE STIFFNESS

This section describes the application of the SLA to predict the tensile stiffness of HexMC. As discussed in section 2.1, the SLA involves modeling a structure in terms of RLVEs, in which each RLVE can be viewed as a continuous-fiber laminate. Stacking sequence varies discontinuously from one RLVE to the next. The predicted elastic properties of a single RLVE will be discussed first, because the elastic properties of a single RLVE can be conveniently calculated using classical lamination theory (CLT). Results from the CLT analyses were used to study trends in predicted properties as a function of: (1) the number of iterations and (2) the number of through-thickness chips. These initial calculations ultimately inform studies of structures composed of many RLVEs, which are based on more computationally expensive finite-element analyses.

3.1 ANALYSIS OF A SINGLE RANDOM LAMINATE VOLUME ELEMENT

A single RLVE is shown schematically in figure 4. The stacking sequence is defined by specifying *n* random fiber angles, where *n* equals the number of through-thickness chips. The elastic properties assumed for each chip have been previously listed in table 1. The effective elastic moduli E_{xx}, E_{yy}, ν_{xy}, and G_{xy} of the RLVE are based on midplane values of strain and are given by:

$$E_{xx} = \frac{1}{t(a_{11})} \tag{11}$$

$$E_{yy} = \frac{1}{t(a_{22})} \tag{12}$$

$$\nu_{xy} = \frac{-a_{12}}{a_{11}} \tag{13}$$

$$G_{xy} = \frac{1}{t(a_{66})} \tag{14}$$

where t = thickness of the RLVE and a_{11}, a_{12}, a_{22}, and a_{66} are elements of the compliance matrix for a laminated plate [20]. Because a new set of chip fiber angles (θ_n) is selected during each iteration, all of the elastic properties of the RLVE vary with each iteration.

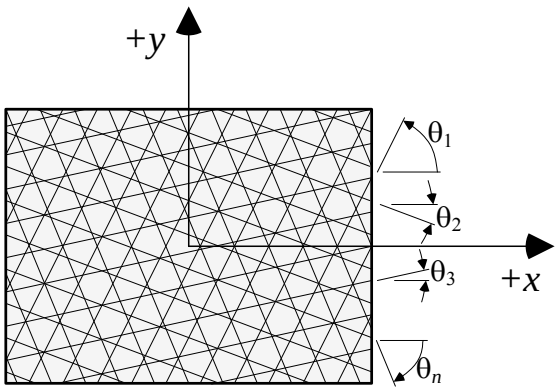

Figure 4. Schematic representation of a single RLVE, indicating *n* random chip orientations

An RLVE with eight through-thickness chips was considered first. Properties based on up to 1500 iterations are summarized in table 3 and plotted in figures 5–8. Mean (average) values, standard deviations, maximum values, and minimum values are all included. Note that, because the analyses are based on randomly-selected fiber angles, different values would be obtained if these analyses were repeated, especially at low numbers of iterations. However, average and standard deviations tend toward constant values following approximately 150 iterations. Though not described here, the average and standard deviations listed in table 3 differed by less than 2% if the number of iterations was increased to 3000. Therefore, it was concluded that 1500 iterations were sufficient to identify trends in predicted properties.

Table 3. Predicted properties of a single 8-chip RLVE as a function of number of iterations

Number of Iterations	Predicted E_{xx}, GPa (Msi)				Predicted E_{yy}, GPa (Msi)			
	Mean	Standard Deviation	Maximum Value	Minimum Value	Mean	Standard Deviation	Maximum Value	Minimum Value
50	32.86 (4.77)	12.40 (1.80)	59.60 (8.64)	11.02 (1.60)	36.17 (5.25)	12.20 (1.77)	64.39 (9.34)	12.64 (1.83)
150	34.39 (4.99)	12.70 (1.84)	73.98 (10.7)	11.02 (1.60)	33.50 (4.86)	12.20 (1.77)	67.60 (9.80)	12.64 (1.83)
300	34.31 (4.98)	12.71 (1.84)	75.77 (11.0)	11.02 (1.60)	33.62 (4.88)	12.51 (1.82)	69.09 (10.0)	11.22 (1.63)
600	34.62 (5.02)	12.87 (1.87)	75.77 (11.0)	9.93 (1.44)	34.14 (4.95)	13.10 (1.90)	85.98 (12.5)	11.22 (1.63)
900	34.83 (5.05)	13.02 (1.89)	75.77 (11.0)	9.93 (1.44)	34.01 (4.93)	12.95 (1.88)	85.98 (12.5)	9.34 (1.36)
1200	34.85 (5.06)	13.16 (1.91)	98.80 (14.3)	9.93 (1.44)	34.22 (4.96)	13.08 (1.90)	85.98 (12.5)	9.18 (1.33)
1500	35.11 (5.09)	13.31 (1.93)	98.80 (14.3)	9.93 (1.44)	34.33 (4.98)	13.00 (1.89)	85.98 (12.5)	9.18 (1.33)

Number of Iterations	Predicted ν_{xy}				Predicted G_{xy}, GPa (Msi)			
	Mean	Standard Deviation	Maximum Value	Minimum Value	Mean	Standard Deviation	Maximum Value	Minimum Value
50	0.287	0.178	0.868	-0.081	12.05 (1.75)	2.946 (0.427)	20.37 (2.95)	6.487 (0.941)
150	0.304	0.171	0.868	-0.081	12.39 (1.79)	3.292 (0.469)	20.73 (2.95)	6.487 (0.941)
300	0.313	0.166	0.868	-0.081	12.67 (1.84)	3.209 (0.465)	21.51 (3.12)	6.487 (0.941)
600	0.317	0.173	0.962	-0.081	12.66 (1.84)	3.290 (0.477)	22.71 (3.29)	6.487 (0.941)
900	0.320	0.177	0.999	-0.081	12.70 (1.84)	3.297 (0.478)	22.99 (3.34)	6.349 (0.921)
1200	0.317	0.181	1.247	-0.081	12.71 (1.84)	3.287 (0.477)	22.99 (3.34)	6.152 (0.892)
1500	0.315	0.184	1.247	-0.122	12.65 (1.84)	3.296 (0.478)	25.30 (3.67)	5.401 (0.783)

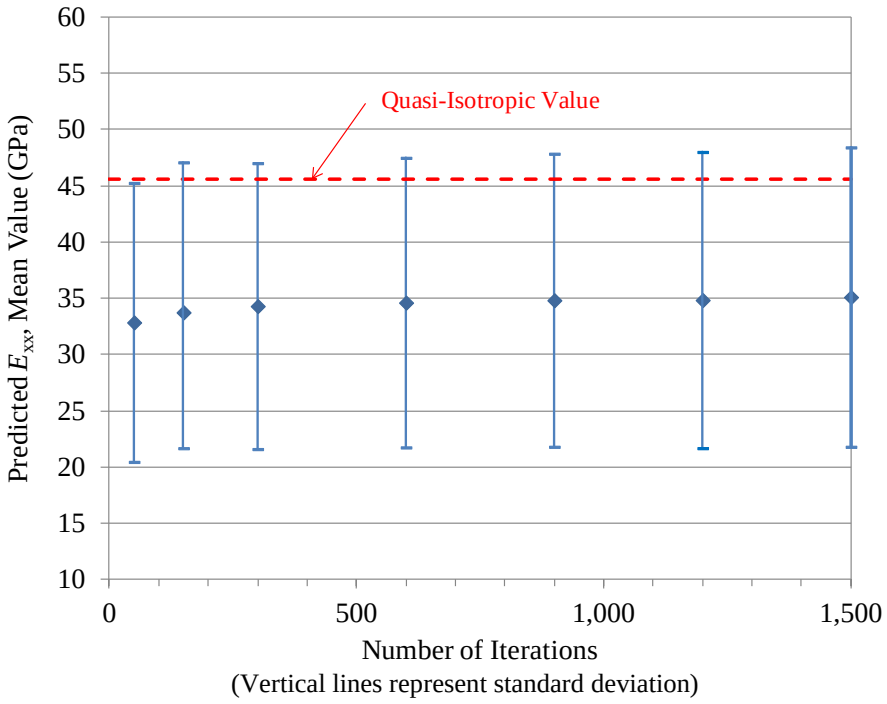

Figure 5. Stiffness E_{xx} predicted for a single eight-chip RLVE as a function of iterations

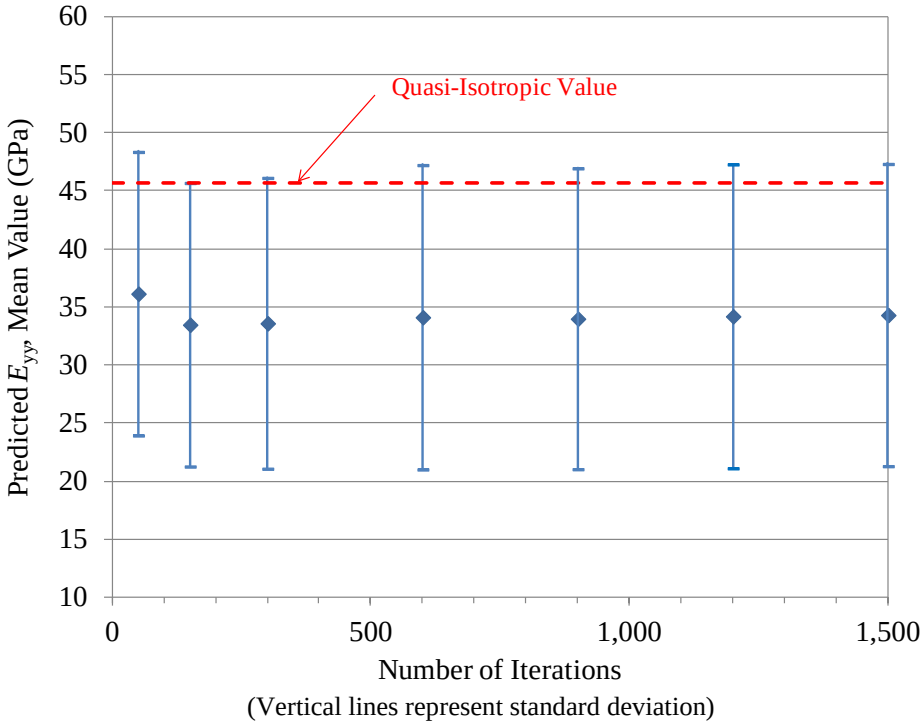

Figure 6. Stiffness E_{yy} predicted for a single eight-chip RLVE as a function of iterations

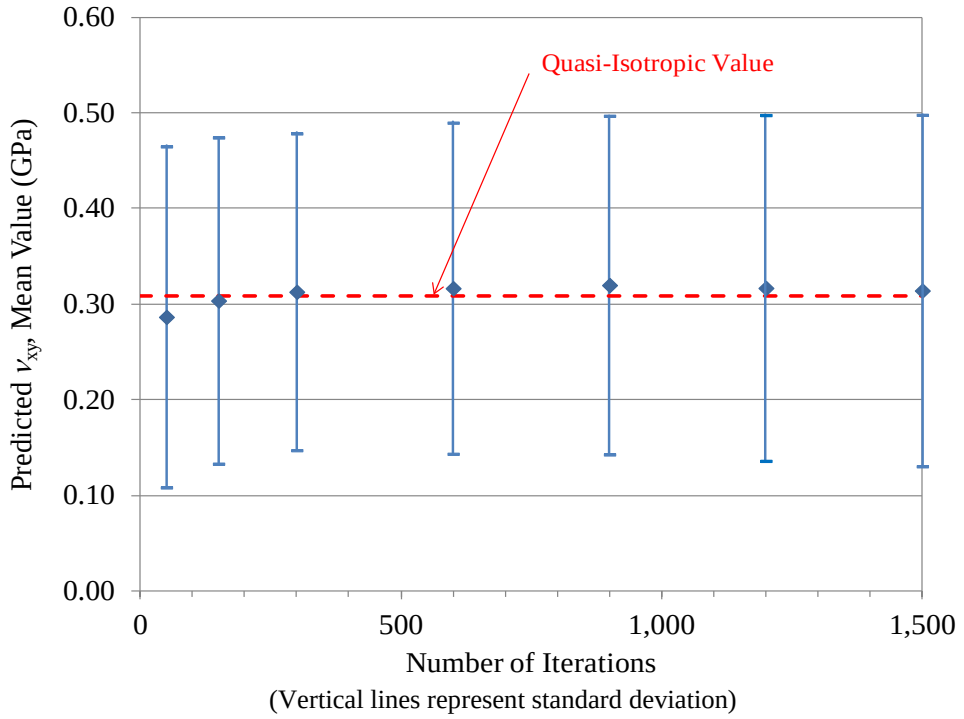

Figure 7. Poisson ratio ν_{xy} predicted for a single eight-chip RLVE as a function of iterations

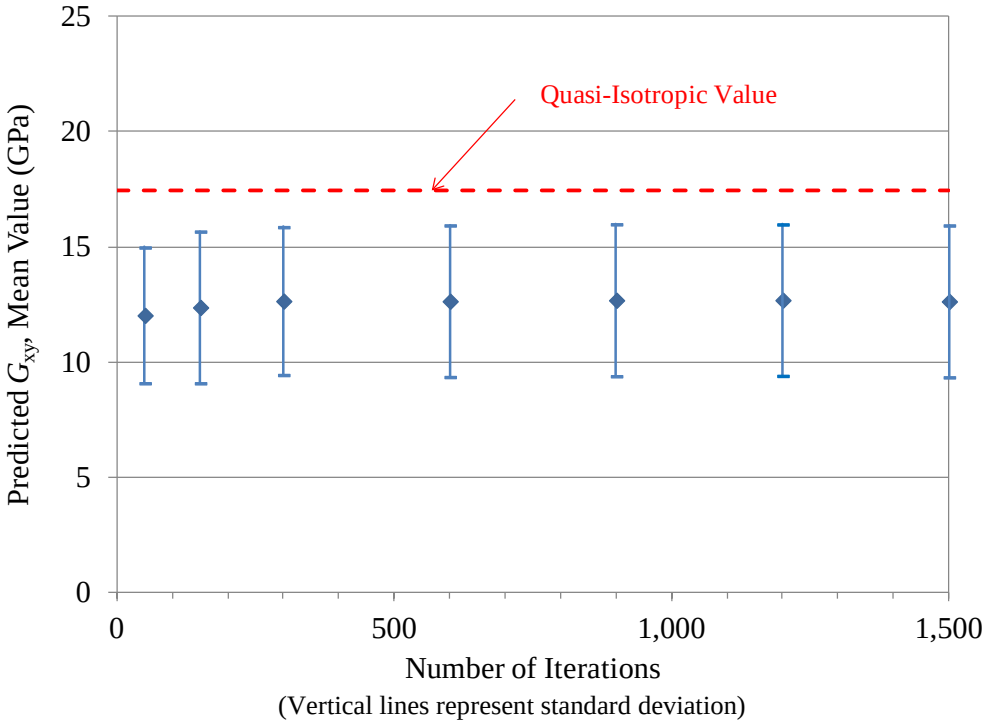

Figure 8. Shear stiffness G_{xy} predicted for a single eight-chip RLVE as a function of iterations

The elastic properties of a quasi-isotropic laminate produced using plies with the properties listed in table 1 can be shown to be [20]:

$$E_{xx}^{quasi} = E_{yy}^{quasi} = 45.62\,GPa \;\; (6.62\,\text{Msi})$$

$$\nu_{xy}^{quasi} = 0.309$$

$$G_{xy}^{quasi} = 17.43\,GPa \;\; (2.53\,\text{Msi})$$

Quasi-isotropic values were included in figures 5–8. The figures show that mean properties predicted for an eight-chip RLVE differ substantially from quasi-isotropic values. In particular, mean values of in-plane stiffnesses E_{xx}, E_{yy}, and G_{xy} are substantially below quasi-isotropic values for an eight-chip RLVE.

Recall that the coefficient of variation (CoV) is defined as:

$$CoV = \left(\frac{\text{Standard Deviation}}{\text{Mean}} \right) x100\%$$

The results presented in table 3 imply that for an eight-chip RLVE, the predicted *CoV* for E_{xx}, E_{yy}, ν_{xy}, and G_{xy} is approximately 38%, 38%, 58%, and 26%, respectively, based on 1500 iterations.

Similar analyses were performed for RLVEs with an increased number of chips. The mean properties calculated as the number of chips are increased (or equivalently, as overall thickness is increased) are presented in table 4 and plotted in figures 9–12. All of these values are based on 1500 iterations at each thickness. Standard deviations, maximum values, and minimum values are included. Two trends are immediately apparent. First, as the number of through-thickness chips is increased, the average values of all three in-plane stiffnesses (E_{xx}, E_{yy}, and G_{xy}) increase and approach the quasi-isotropic values. Second, as the number of through-thickness chips is increased, the standard deviation is decreased. Nevertheless, significant variations in properties persist even for large numbers of through-thickness chips. For example, for the case of 74 through-thickness chips, the in-plane stiffness E_{xx} (or E_{yy}) is expected to exhibit a CoV of approximately 10%.

Table 4. Predicted properties of a single RLVE as a function of number of chips, based on 1500 iterations

Thickness, mm (in)	No. of Chips	Predicted E_{xx}, GPa (Msi)				Predicted E_{yy}, GPa (Msi)			
		Mean	Standard Deviation	Maximum Value	Minimum Value	Mean	Standard Deviation	Maximum Value	Minimum Value
1.02 (0.04)	8	35.11 (5.09)	13.31 (1.93)	98.80 (14.3)	9.93 (1.44)	34.33 (4.98)	13.00 (1.89)	85.98 (12.5)	9.18 (1.33)
1.52 (0.06)	12	38.28 (5.55)	11.07 (1.61)	75.77 (11.0)	9.09 (1.32)	38.28 (5.55)	11.49 (1.67)	79.63 (11.6)	11.85 (1.72)
2.03 (0.08)	16	40.17 (5.83)	9.75 (1.41)	70.26 (10.2)	15.02 (2.18)	40.67 (5.90)	9.67 (1.40)	70.46 (10.2)	13.67 (1.98)
2.30 (0.09)	18	41.10 (5.96)	9.27 (1.34)	81.22 (11.8)	14.77 (2.14)	40.64 (5.89)	9.09 (1.32)	73.98 (10.7)	15.61 (2.26)
3.05 (0.12)	24	41.84 (6.07)	7.79 (1.14)	71.50 (10.4)	21.82 (3.16)	42.37 (6.14)	8.19 (1.19)	69.22 (10.0)	14.92 (2.16)
4.06 (0.16)	32	43.02 (6.24)	7.31 (1.06)	73.43 (10.6)	18.49 (2.68)	42.95 (6.23	7.07 (1.03)	67.02 (9.72)	21.37 (3.10)
5.80 (0.23)	46	43.82 (6.36)	5.71 (0.828)	61.05 (8.85)	22.27 (3.23)	43.83 (6.36)	5.91 (0.858)	61.78 (8.96)	27.72 (4.02)
9.40 (0.37)	74	44.60 (6.47)	4.59 (0.665)	60.21 (8.73)	29.50 (4.28)	44.33 (6.43)	4.44 (0.645)	63.90 (9.27)	28.94 (4.20)

Thickness, mm (in)	No. of Chips	Predicted ν_{xy}				Predicted G_{xy}, GPa (Msi)			
		Mean	Standard Deviation	Maximum Value	Minimum Value	Mean	Standard Deviation	Maximum Value	Minimum Value
1.02 (0.04)	8	0.315	0.184	1.247	-0.122	12.65 (1.84)	3.30 (0.478)	25.30 (3.67)	5.40 (0.783)
1.52 (0.06)	12	0.302	0.136	0.901	-0.065	14.04 (2.00)	2.91 (0.393)	24.21 (3.01)	6.81 (1.11)
2.03 (0.08)	16	0.304	0.106	0.879	0.005	14.93 (2.16)	2.47 (0.359)	23.00 (3.34)	8.61 (1.25)
2.30 (0.09)	18	0.308	0.102	0.876	0.075	15.24 (2.21)	2.38 (0.322)	23.96 (3.48)	8.32 (1.48)
3.05 (0.12)	24	0.306	0.084	0.722	0.067	15.76 (2.29)	2.02 (0.293)	21.82 (3.16)	8.96 (1.30)
4.06 (0.16)	32	0.309	0.069	0.576	0.121	16.19 (2.35)	1.68 (0.244)	22.00 (3.19)	10.71 (1.55)
5.80 (0.23)	46	0.308	0.054	0.531	0.162	16.55 (2.40)	1.38 (0.200)	20.84 (3.02)	12.12 (1.76)
9.40 (0.37)	74	0.310	0.041	0.506	0.190	16.93 (2.46)	1.12 (0.162)	20.74 (3.01)	13.13 (1.90)

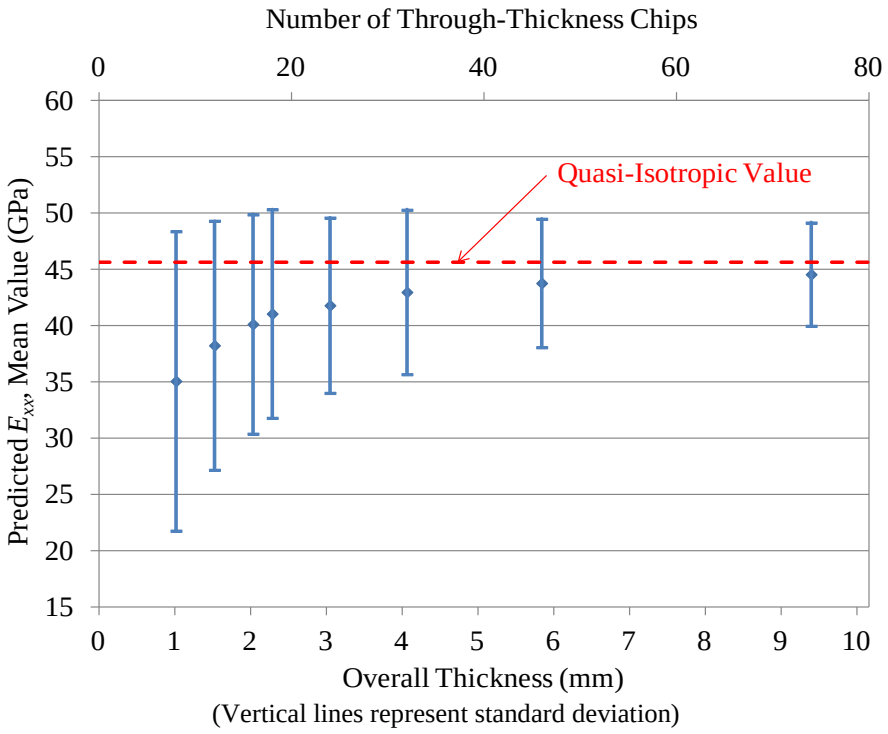

Figure 9. Stiffness E_{xx} predicted for a single RLVE as a function of thickness

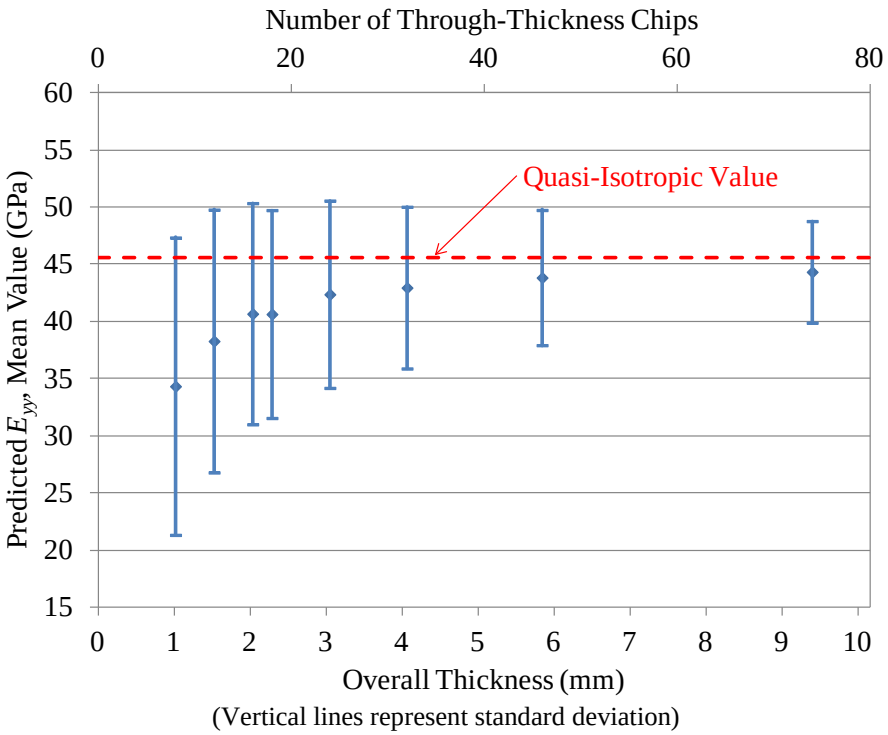

Figure 10. Stiffness E_{yy} predicted for a single RLVE as a function of thickness

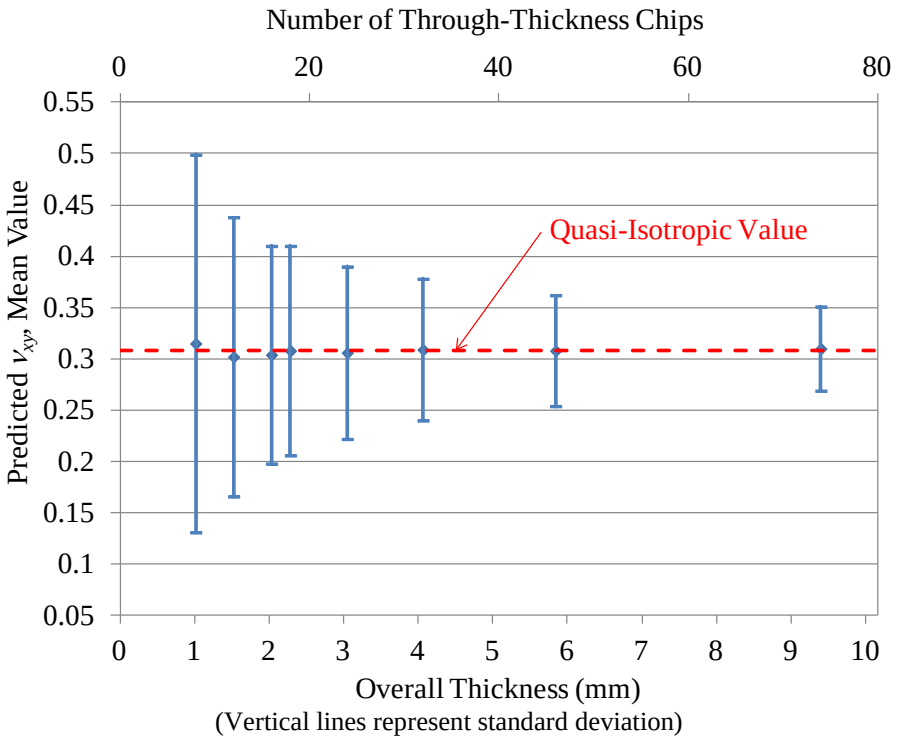

Figure 11. Poisson ratio ν_{xy} predicted for a single RLVE as a function of thickness

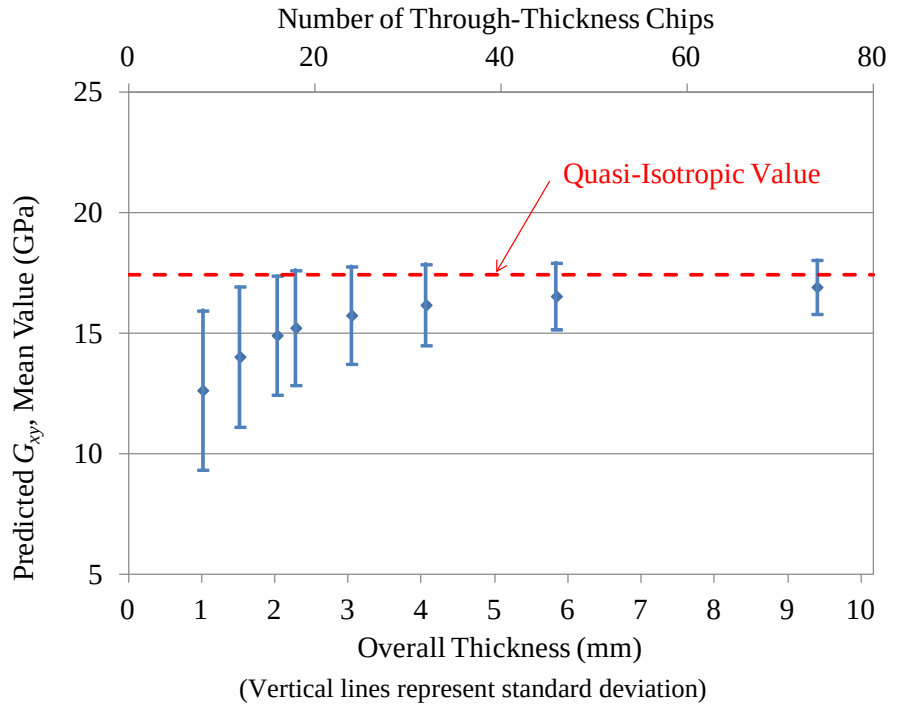

Figure 12. Shear stiffness G_{xy} predicted for a single RLVE as a function of thickness

3.2 PREDICTED HEXMC STIFFNESSES

As discussed in section 2.1, the first step in applying the SLA is to divide the structure of interest into RLVEs. In this section, the SLA will be used to predict the tensile stiffness of a HexMC tensile specimen. All specimens considered had a width and length of 38 mm and 305 mm (1.5 in and 12 in), respectively. Seven different specimen thicknesses were considered to determine whether the number of through-thickness chips had an impact on predicted elastic modulus. The thicknesses considered, and the corresponding number of chips, is presented in table 5. Each chip was assumed to have a thickness of 0.127 mm (0.005 in), so overall specimen thicknesses were an integer number of chip thicknesses.

Table 5. Assumed thickness of finite element analysis tensile specimen analyses

Number of Chips	Overall Thickness
8	1.02 mm (0.040 in)
16	2.03 mm (0.080 in)
18	2.29 mm (0.090 in)
24	3.05 mm (0.120 in)
32	4.06 mm (0.160 in)
46	5.84 mm (0.230 in)
74	9.40 mm (0.370 in)

The predictions generated during this study were compared to proprietary database generated by the Hexcel Corporation. Nominal in-plane dimensions of the tensile specimens used during Hexcel studies were 38 mm x 305 mm (1.5 in x 12 in). Therefore, the FE models in this study were based on these dimensions as well. As discussed in section 2.1, RLVEs with nominal in-plane dimensions of 19 mm x 19mm (0.75in x 0.75 in) were to be used. Therefore, the tensile specimens were modeled using 2 RLVEs in width and 16 RLVEs in length. A sketch showing the RLVEs used to model the specimens is shown in figure 13. Specimen geometry was first defined as a CAD model using SOLIDWORKS and then imported into Femap for preprocessing. A mid-surface model was created and discretized into 32 RLVEs using Femap. Unique fiber angles were randomly generated for each RLVE. The number of fiber angles generated corresponded to the number of chips and, therefore, to the overall thickness of the specimen. For example, a 1.02-mm- (0.040 in) thick specimen was modeled with eight through-thickness chips; therefore, in this case, eight random fiber angles were generated for each RLVE.

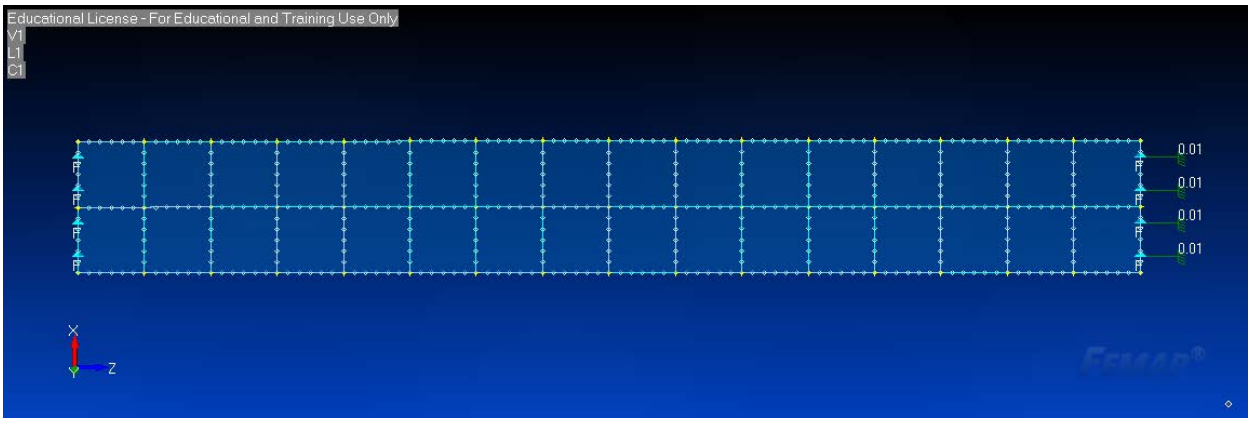

Figure 13. The RLVEs used to define a 38mm x 305 mm tensile specimen

Once the RLVEs were defined, a finite-element mesh was generated, as shown in figure 14. As discussed in section 2.1, each RLVE contained 36 finite elements. The total number of elements used was 1152 (32 RLVEs x 36 element/RLVE). All elements within a given RLVE are defined with the stacking sequence assigned to the RLVE as a whole. Because 32 RLVEs were used, each analysis involved 32 randomly generated stacking sequences.

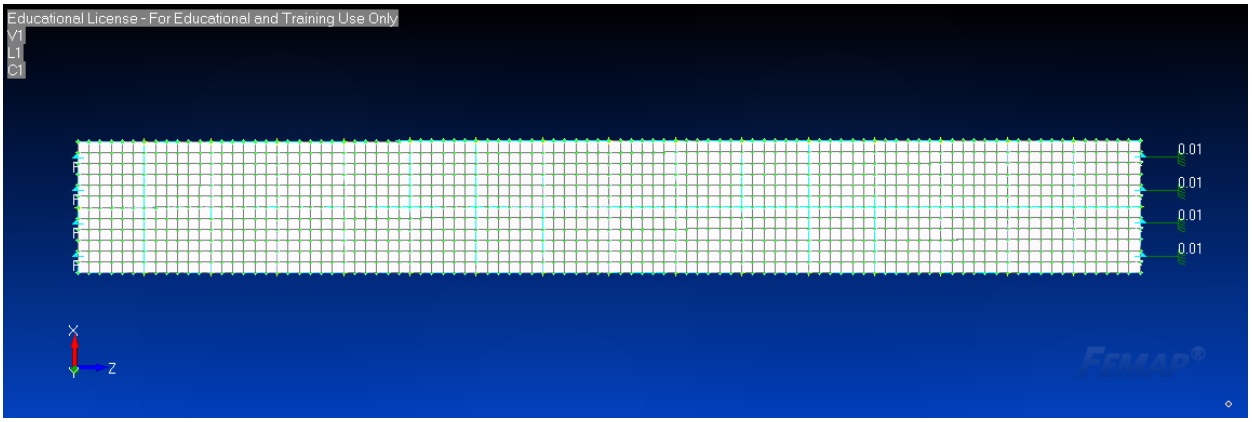

(RLVE boundaries indicated by light blue lines)

Figure 14. Finite-element mesh used to model a 38 mm x 305 mm tensile specimen

To simulate uniaxial tensile loading, all nodes on the left edge shown in figure 14 were fixed in the axial direction (i.e., nodes along the left edge were fixed in the horizontal direction), whereas an enforced axial end displacement of 0.254 mm (0.01 in) was applied to all the nodes on the right edge. Because the overall specimen length was 305 mm (12 in), the enforced uniform end displacement corresponds to an overall axial strain ε_{ax} = (0.254mm/305mm) = 833 $\mu\varepsilon$. Reaction forces at each of the fixed nodes along the left edge were predicted during the finite element model (FEM) analysis. The sum of all axial reaction forces (e.g., ΣR) equals the total axial load induced in the specimen. The nominal axial stress was calculated by dividing the sum of reaction forces by the specimen cross-sectional area, $\sigma_{ax} = \Sigma R/A$. The predicted overall stress-strain curve could then be calculated, and the slope of that curve represents the predicted nominal elastic modulus of a HexMC specimen ($E = \sigma_{ax}/\varepsilon_{ax}$). A total of 1500 separate analyses were performed

for each of the seven specimen thicknesses listed in table 5. Because fiber orientations were varied randomly for all RLVEs from one analysis to the next, 1500 different stress-strain curves were predicted for each thickness. For example, the first 150 tensile stress-strain curves predicted for 1.02-mm-thick specimens (i.e., specimens with eight through-thickness chips) are plotted together in figure 15. It is apparent that the predicted elastic modulus for HexMC exhibits a relatively high variability, in qualitative agreement with experimentally measured stiffness values [6].

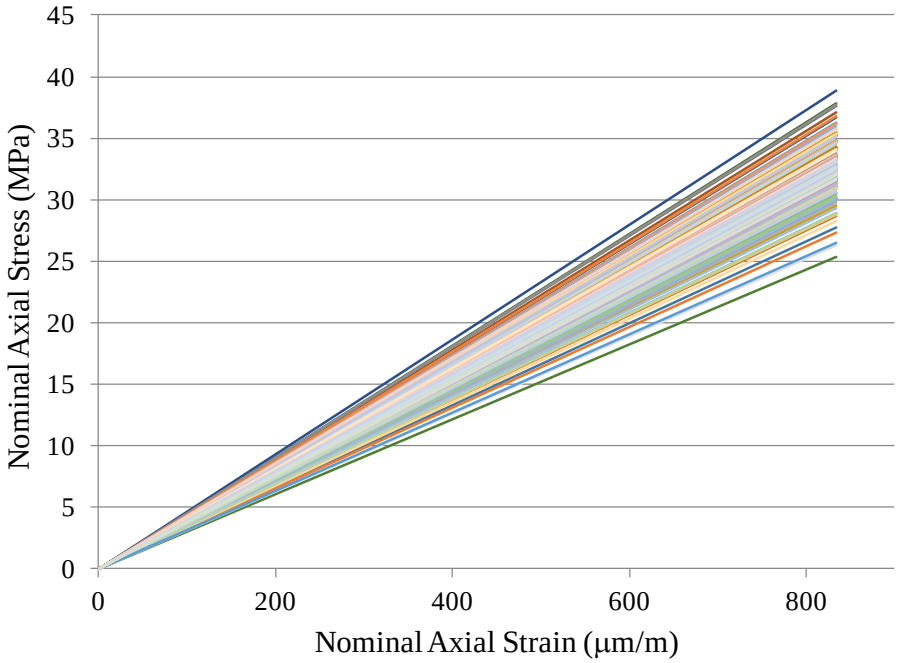

Figure 15. Stress-strain curves predicted during 150 separate analyses for a 1.02-mm-thick HexMC tensile specimen

The mean and standard deviation of predicted stiffness for each thickness are included in table 6 and plotted in figure 16. Based on 1500 analyses, it is apparent that, as specimen thickness is increased, the predicted mean stiffness is increased, whereas the standard deviation is decreased. These trends are in qualitative agreement with the preliminary CLT calculations discussed in section 3.1. However, unlike the CLT analysis, the predicted mean stiffness does not converge to the quasi-isotropic value as the number of chips is increased. Instead, the mean stiffness for specimens with 24 through-thickness chips or more converges to approximately 42 GPa. Recall that the quasi-isotropic stiffness is 45.62 GPa. Therefore, it is seen that SLA analyses predicts a mean HexMC stiffness of approximately 92% of the quasi-isotropic value, with a CoV of approximately 18%. This is in excellent agreement with results reported elsewhere, as reported values of HexMC stiffness range from 90% [21] to 100% [15] of the corresponding quasi-isotropic value.

Table 6. Mean and standard deviation of the predicted HexMC elastic modulus over a range of thicknesses, based on 1500 SLA analyses for each thickness

Specimen Thickness	Number of Chips	Predicted Elastic Modulus			
		Mean	Standard Deviation	Maximum Value	Minimum Value
1.02 mm (0.04 in)	8	36.18 GPa (5.25 Msi)	2.56 GPa (0.371 Msi)	46.06 GPa (6.68 Msi)	27.13 GPa (3.94 Msi)
2.03 mm (0.08 in)	16	40.66 GPa (5.90 Msi)	1.78 GPa (0.259 Msi)	47.56 GPa (6.90 Msi)	33.23 GPa (4.82 Msi)
2.30 mm (0.09 in)	18	41.05 GPa (5.95 Msi)	1.69 GPa (0.245 Msi)	46.04 GPa (6.68 Msi)	35.25 GPa (5.11 Msi)
3.05 mm (0.120in)	24	41.87 GPa (6.07 Msi)	1.429 GPa (0.207 Msi)	46.83 GPa (6.79 Msi)	37.32 GPa (5.41 Msi)
4.06 mm (0.160in)	32	42.28 GPa (6.13 Msi)	1.251 GPa (0.181 Msi)	46.99 GPa (6.82 Msi)	38.60 GPa (5.60 Msi)
5.80 mm (0.23 in)	46	42.40 GPa (6.15 Msi)	0.98 GPa (0.143 Msi)	45.22 GPa (6.56 Msi)	39.08 GPa (5.67 Msi)
9.40 mm (0.37 in)	74	41.95 GPa (6.08 Msi)	0.773GPa (0.112 Msi)	44.80 GPa (6.50 Msi)	39.68 GPa (5.76 Msi)

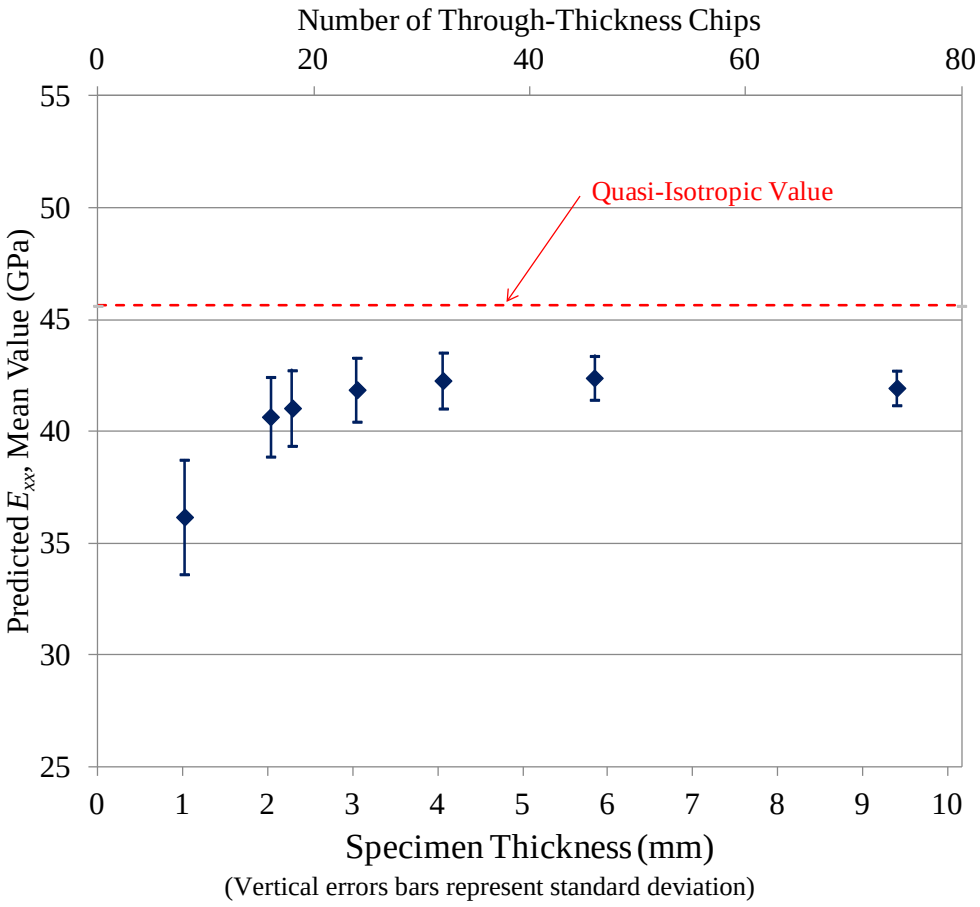

Figure 16. Predicted mean stiffness as a function of specimen thickness, based on 1500 analyses for each thickness

A visual check was performed for each thickness to determine if predicted stiffness values follow a normal (i.e., Gaussian) distribution. Individual predicted stiffness values were first divided by the mean stiffness, such that the normalized data has a mean value of 1.0. Predictions for each thickness were then arranged in ascending order, and the probability of survival at each value was computed using equation (4). The distribution of predicted stiffness values for a 1.02-mm-thick specimen is compared with a normal (i.e., Gaussian) distribution in figure 17. As can be seen, the predicted values and Gaussian distribution curve are essentially coincident. Similarly, good agreement was obtained for all thicknesses considered during this study.

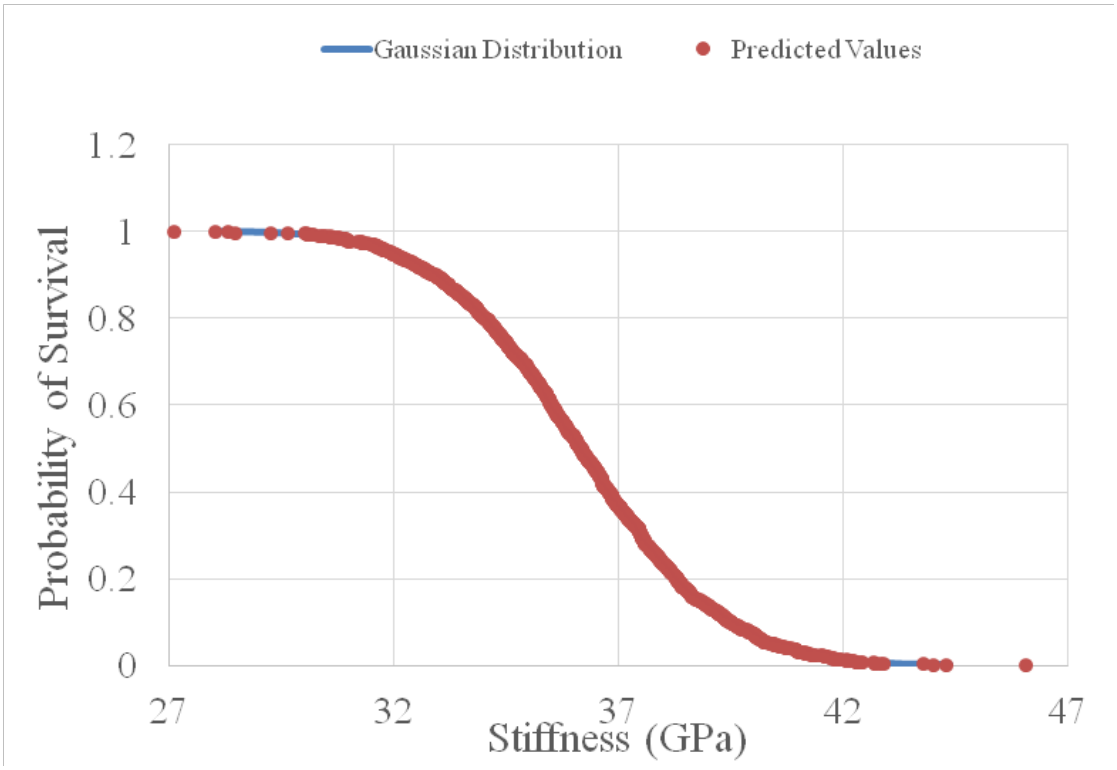

Figure 17. Comparison between predicted stiffness of a 1.02-mm-thick specimen and a standard normal distribution

Finally, the tolerance factor k_b was calculated using equations (5)–(8), and the B-basis and Bmax stiffness values were calculated using equations (9) and (10), respectively. Predicted B-basis and Bmax stiffness values are presented as a function of thickness in table 7 and plotted in figure 18. As has been previously shown in figure 16, the mean elastic stiffness is predicted to remain essentially constant for specimens with a thickness greater than approximately 0.120 mm (24 through-thickness chips), but the standard deviation is predicted to decrease. The steady increase in predicted B-basis values and steady decrease in Bmax values as shown in figure 18 are due to decreasing values of standard deviation as thickness is increased.

Table 7. Predicted B-basis, average, and Bmax HexMC stiffness values

Specimen Thickness	B-basis Stiffness	Average Stiffness	Bmax Stiffness
1.02 mm (0.04 in)	32.79 GPa (4.76 Msi)	36.18 GPa (5.25 Msi)	39.57 GPa (5.74 Msi)
2.03 mm (0.08 in)	38.29 GPa (5.55 Msi)	40.66 GPa (5.90 Msi)	43.02 GPa (6.24 Msi)
2.30 mm (0.09 in)	38.81 GPa (5.63 Msi)	41.05 GPa (5.95 Msi)	43.29 GPa (6.28 Msi)
3.05 mm (0.120 in)	39.98 GPa (5.80 Msi)	41.87 GPa (6.07 Msi)	43.76 GPa (6.35 Msi)
4.06 mm (0.160 in)	40.62 GPa (5.89 Msi)	42.28 GPa (6.13 Msi)	43.94 GPa (6.37 Msi)
5.80 mm (0.23 in)	41.10 GPa (5.96 Msi)	42.40 GPa (6.15 Msi)	43.71 GPa (6.34 Msi)
09.4 mm (0.37 in)	40.88 GPa (5.93 Msi)	41.92 GPa (6.08 Msi)	42.95 GPa (6.23 Msi)

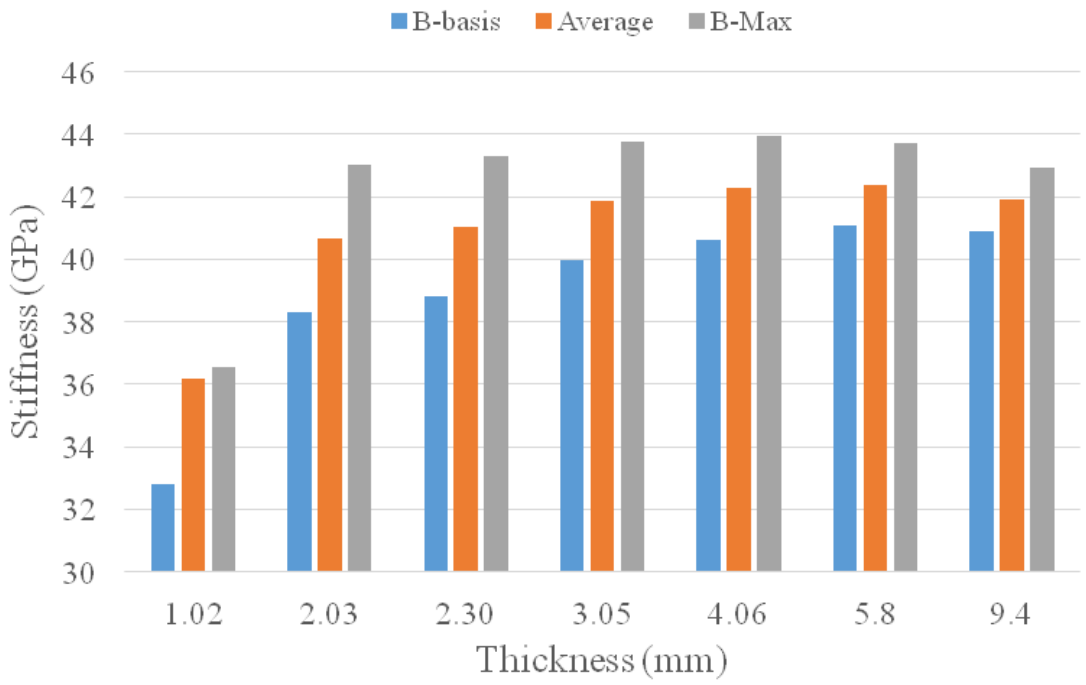

Figure 18. Predicted Bmax, average, and B-basis stiffness values of HexMC

A proprietary HexMC database generated by the Hexcel Corporation was made available to the authors during this study. The data include 18 stiffness values measured at four specimen thicknesses: 2.3 mm, 3.6 mm, 5.8 mm, and 9.4 mm. The mean, B-basis, and Bmax stiffness values based on these measurements were calculated at the University of Washington (UW). A

comparison of normalized predicted and measured stiffness values is shown in figure 19. Agreement between measurement and prediction is reasonable in the sense that both measured and predicted mean values remain essentially constant over the thicknesses tested by Hexcel. Note that the Hexcel B-basis and Bmax stiffness values are based on only 18 data points at the four thicknesses considered, whereas the UW-predicted values are based on 1500 simulations at seven specimen thicknesses. The difference between the B-basis and Bmax stiffnesses measured by Hexcel would likely decrease if a greater number of measurements were available.

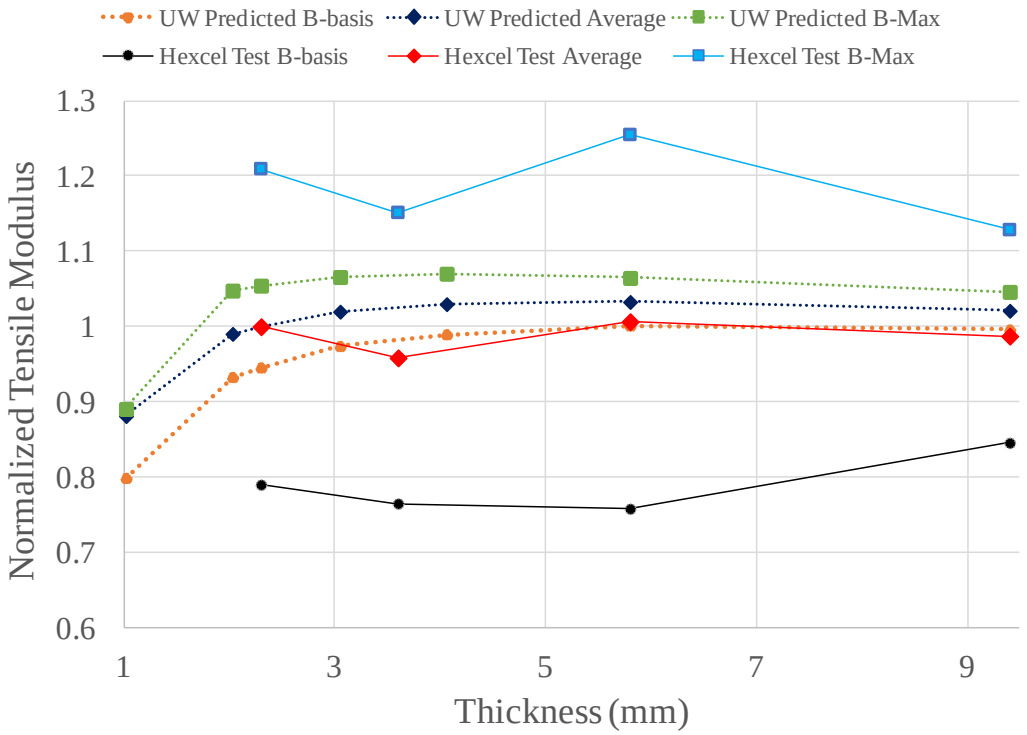

(Both the Hexcel measurements and UW predictions are normalized to mean values for 2.3-mm-thick specimens)

Figure 19. Comparison between measured and predicted tensile moduli

4. STRENGTH PREDICTIONS

Strength predictions of HexMC unnotched and open-hole tensile specimens were obtained by combining the SLA, described in section 2.1, and a simple damage accumulation model applied to each finite element. The damage accumulation model used is often called the “ply discount” scheme. A flowchart summarizing individual steps is shown in figure 20. The following discussion refers to the individual steps listed in the figure.

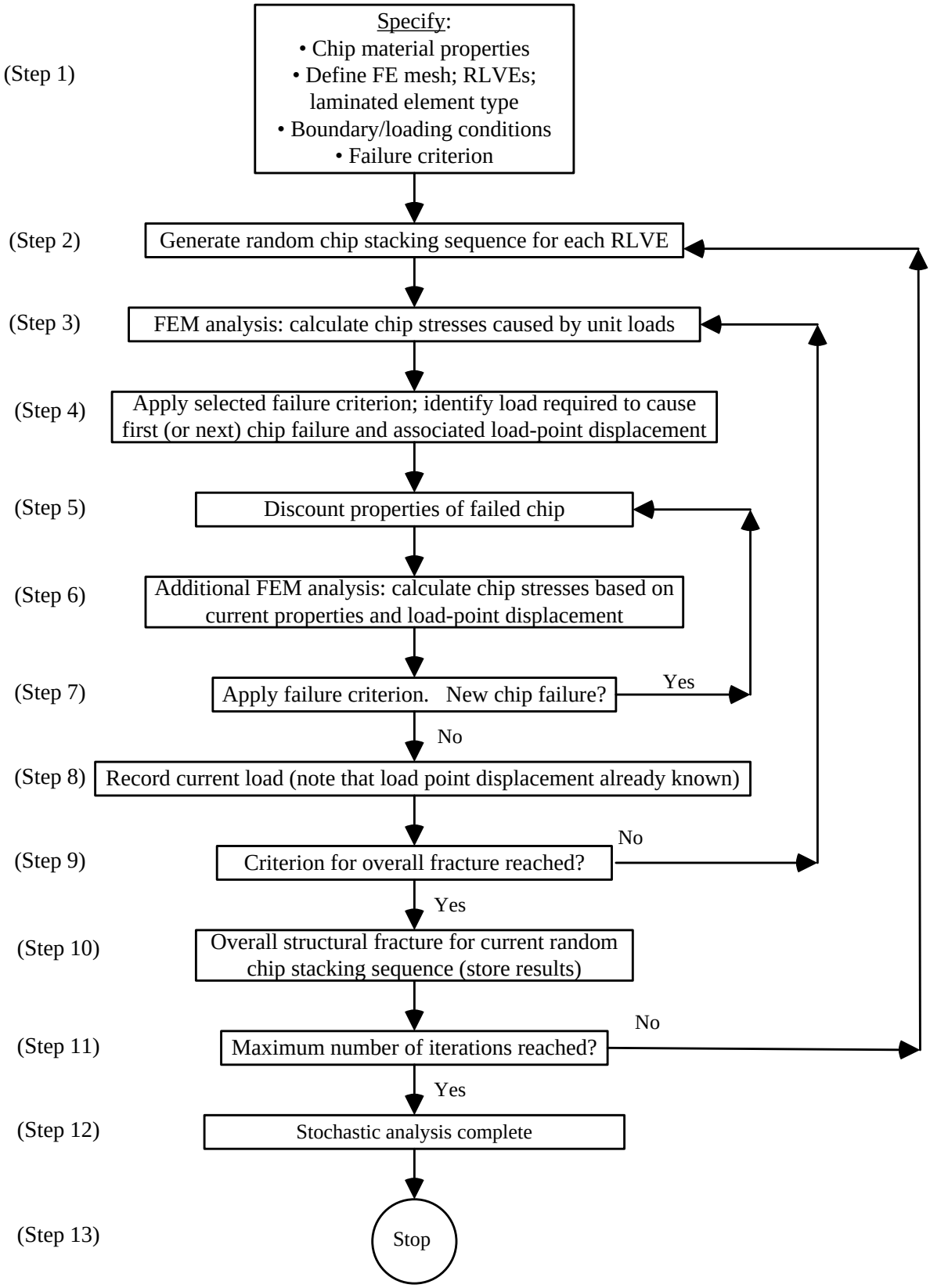

Figure 20. Flow chart of the combined SLA and ply discount scheme

Step 1 is to define the problem. That is, to specify all required material properties, create a finite-element mesh representing the structure of interest, the type of laminated finite element to be used, the boundary conditions, and the ply failure criterion to be used. In this study, numerical CAD models of unnotched and open-hole tension specimens were first generated using SOLIDWORKS and then imported to Femap for pre- and post-processing. Laminated shell elements were used in all analyses and NX Nastran was used as the finite-element solver. The Tsai-Wu failure criterion was selected for use, primarily because this criterion is available in NX Nastran and could, therefore, be readily applied.

Step 2 is to generate a random chip stacking sequence for each RLVE. A Visual Basic® code was written to generate random angles ranging from -90° to 90° for each RLVE. As described in section 2.1, the stacking sequence of a given RLVE is completely independent of the stacking sequence in neighboring RLVEs, and the stacking sequence of an individual finite element is dictated by the RLVE in which the element resides. Repeated analyses of the HexMC structure, where new random stacking sequences are generated for all RLVEs by the Visual Basic code and transferred to the NX Nastran solver via Femap during each analysis, captures the variable stiffness and strengths exhibited by HexMC structures.

In step 3, unit loads (or unit displacements) are applied to the finite element model in accordance with the boundary conditions defined in step 1. Therefore, the stresses caused in each ply/chip of each element by a unit load or unit displacement are determined.

In step 4, the ply/chip closest to failure, as predicted by the selected failure criterion, is identified, and the increase in unit loading required to cause the first (or next) ply/chip failure is determined. The Tsai-Wu failure criterion is available in NX Nastran and was used during this study. Therefore, in this step, the increase in loading necessary to cause the Tsai-Wu failure index to precisely equal 1 for the ply/chip nearest to failure was determined.

In step 5, the elastic properties for the failed ply/chip are reduced (i.e., properties of the failed chip are “discounted”). Specifically, once a chip is predicted to fail, the fiber-dominated modulus (E_{11}) is reduced to 90% of the original value, whereas the matrix-dominated moduli (E_{22} and G_{12}) are reduced to 30% of the original values. Poisson’s ratio is not changed. Referring to the elastic properties for AS4/8552 previously listed in table 1, in the present study the elastic properties of failed chips were reduced to E_{11} = 106 GPa, E_{22} = 2.4 GPa, and G_{12} = 1.34 GPa, and Poisson’s ratio was maintained at ν_{12} = 0.32. Note that the percentage decreases in elastic moduli used in this study are thought to be reasonable for graphite-epoxy composites, but admittedly they were selected arbitrarily.

Failure of a chip will cause redistribution of stresses and strains in regions near the failed chip. This implies that a chip failure may precipitate additional chips failures without any change in external displacements. Consequently, in step 6, a new FEM analyses is performed based on the prevailing external loads/displacements and using discounted properties for the newly failed ply. Results from the additional FEM analysis are then used to determine if any additional chip failures are predicted (step 7) at the current load/displacement level. Additional chip failures often do occur, but they rarely occur in the same finite element. Rather, additional chip failures are typically predicted for other elements dispersed within the model. This shows that the SLA

approach holds great promise in modeling HexMC materials and structures, because experimental measurements have shown that this is how dispersed damage accumulates [7, 13].

Steps 5–7 are iterated until no new chip failures are predicted at the current external load/displacement level. Once no additional ply failures are predicted, the load and displacements are stored in an Excel file (step 8) for subsequent data reduction.

To this point the predicted chip failures represent the accumulation of damage within the structure. A single (or multiple) chip failure(s) does not necessarily cause overall structural fracture. In step 9, a criterion representing overall fracture of the structure must be evaluated.

The following four different structural fracture criteria were considered during this study:

1. Fracture is declared when all chips within a single finite element have failed.
2. Fracture is declared when a preselected number of chips throughout the model have failed (e.g., when 2000 chips have failed).
3. Fracture is declared when the effective stiffness of the structure has decreased by some preselected amount (e.g., when overall stiffness has reduced by 15%).
4. Fracture is declared when all chips in all finite elements have failed.

Fracture criteria 1 and 4 are well-defined in a mathematical sense and require no further interpretation. However, fracture criterion 1 may often be too conservative, whereas criterion 4 is likely to be too non-conservative. Conversely, fracture criteria 2 and 3 depend on context and require engineering judgment to properly apply. For example, in criterion 2, the user must preselect the number of failed chips that represent fracture. A universal number of failures cannot be defined, however: For example, it is inconsistent to define fracture following 2000 chip failures if only 1500 chips exist in the model. Criterion 3 requires the user to define fracture as a preselected reduction in stiffness. Again, an acceptable reduction in stiffness will depend on the structure under consideration and requires engineering judgment to define.

Another aspect is computational expense. The number of separate finite-element analyses required during a single fracture analysis equals the number of predicted chip failures. Hundreds or thousands of chips failures are predicted during a typical fracture analysis and, therefore, a single fracture analysis may require tens of hours to complete using a typical desktop computer. As hundreds of analyses are desired to predict B-basis strengths, computation times can quickly become prohibitive. Referring to the four fracture criteria listed above, computational expense generally increases in the order listed. Criterion 1 (i.e., fracture is declared when all chips in a single element have failed) is generally the least computationally expensive approach, whereas criterion 4 (i.e., fracture declared when all chips in all elements in the model have failed) requires the greatest computational expense.

Predicted fracture strengths for unnotched and open-hole HexMC tensile specimens are presented in sections 4.1 and 4.2. Most of the analyses presented will be based on fracture criterion 1, though a few analyses based on fracture criterion 4 are also presented to demonstrate the substantial increase in required computational times.

Step 10 is reached when the fracture criterion is satisfied (i.e., when the predicted fracture strength for the current random stacking sequence has been calculated).

The SLA is complete if the maximum number of iterations has been reached (step 11). Conceptually, the number of iterations can be as few as two, as B-basis strengths can be calculated using only two strength values [18]. In practice, it is far more common to base B-basis strengths based on tens or hundreds of experimental measurements.

During the present study, the number of iterations used to simulate B-basis strengths was severely limited because of the computational expense involved. The process used during this study involved four separate software packages: A Visual Basic program written in-house was used to generate random fiber angles for all RLVEs and to generally control the flow of computations depicted in the flow diagram shown in figure 20. Femap was used to condition all input variables for subsequent transfer to the NX Nastran solver, and selected output was stored in Excel files for subsequent data reduction, interpretation, and plotting. Ultimately, tens of hours of computation were required for each fracture analysis. The transfer of information to/from the different software packages added to total computation times. A recommended area for future study is to combine these separate functions into a single standalone software package, which may substantially reduce total computation times.

4.1 UNNOTCHED TENSILE STRENGTH

The initial strength predictions for unnotched tensile specimens were obtained following the process shown in figure 20 and the FEM shown in figure 14. Initial fracture predictions were based on criterion 1, the least computationally expensive option. Nevertheless, it was immediately apparent that if the original finite-element mesh shown in figure 14 was used, then computational times would be prohibitive: A single analysis based on the original mesh required more than 15 hours to complete using a typical desktop computer. Consequently, the size of the model was modified to reduce computation times. Specimen length was decreased from 305 mm (12 in) to 178 mm (7 in) while maintaining the specimen width of 38.1 mm (1.5 in). This decreased the number of RLVEs from 32 to 20, and the number of finite elements from 1152 to 720, substantially reducing computation times.

Unnotched tensile strength predictions were performed for four thicknesses: 1.02 mm, 2.30 mm, 4.06 mm, and 5.80 mm (0.04 in, 0.09 in, 0.16, and 0.23 in, respectively). These thicknesses correspond to 8, 18, 32, and 46 through-thickness chips, respectively. Five analyses were completed for each thickness, based on fracture criterion 1. Predicted failure strengths are summarized in table 8 and plotted in figure 21. Note that the total number of predicted chip failures prior to fracture ranged from as few as 435 chip failures (for one of the 1.02-mm-thick specimen analyses) to as many as 17,531 chip failures (for one of the 5.80-mm-thick specimen analyses). The number of chip failures is equivalent to the number of finite-element analyses performed. Computational times increased dramatically with specimen thickness, ranging from as low as 1.51 hours to as many as 42.89 hours. The locations of the failed element predicted during the five analyses completed for four different thicknesses are shown in figures 22–25. Locations of predicted element failures were dispersed throughout each specimen, reflecting the distributed nature of predicted chip failures in HexMC structures.

Table 8. Predicted fracture strengths for four specimen thicknesses

Specimen Thickness	Analysis Number	Number of Chip Failures	Computation Time (hours)	Fracture Strength
1.02 mm (0.04 in or 8 chips)	1	699	2.38	91.66 MPa (13.30 ksi)
	2	787	2.61	108.77 MPa (15.78 ksi)
	3	773	2.59	152.87 MPa (22.17 ksi)
	4	494	1.70	109.59 MPa (15.90 ksi)
	5	435	1.51	133.64 MPa (19.38 ksi)
	Average ± St Deviation	638 ± 163	2.26 ± 0.52	119.3 ± 24.0 MPa (17.30 ± 3.48 ksi)
2.29 mm (0.09 in or 18 chips)	1	2278	5.85	170.37 MPa (24.71 ksi)
	2	983	2.69	98.89 MPa (14.34 ksi)
	3	3414	8.79	217.31 MPa (31.52 ksi)
	4	4657	11.74	222.25 MPa (32.23 ksi)
	5	2165	5.43	144.00 MPa (20.89 ksi)
	Average ± St Deviation	2699 ± 1392	6.90 ± 3.46	170.6 ± 51.7 MPa (24.74 ± 7.50 ksi)
4.06 mm (0.16 in or 32 chips)	1	5336	17.14	221.73 MPa (32.16 ksi)
	2	9788	27.85	222.58 MPa (32.29 ksi)
	3	10363	30.99	268.11 MPa (38.89 ksi)
	4	6592	19.62	220.73 MPa (32.02 ksi)
	5	11796	34.94	246.76 MPa (35.79 ksi)
	Average ± St Deviation	8775 ± 2705	26.1 ± 7.54	236.0 ± 21.0 MPa (34.2 ± 3.05 ksi)
5.80 mm (0.23 in or 46 chips)	1	17531	42.89	251 MPa (36.4 ksi)
	2	15158	38.57	239 MPa (34.7 ksi)
	3	4211	10.77	181 MPa (26.2 ksi)
	4	13252	32.83	236 MPa (34.2 ksi)
	5	12215	29.87	205 MPa (29.7 ksi)
	Average ± St Deviation	12473 ± 5043	30.98 ± 12.37	222.4 ± 28.7 MPa (32.3 ± 4.16 ksi)

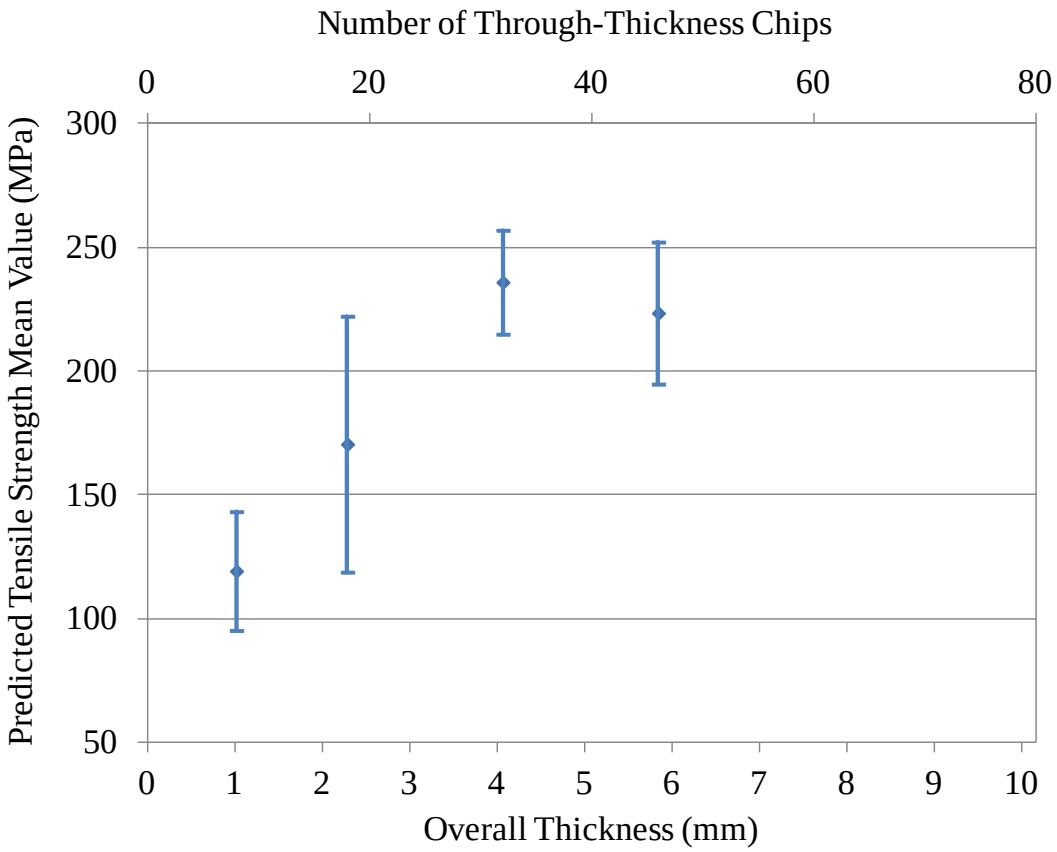

Figure 21. Plot of predicted tensile strength as a function of thickness

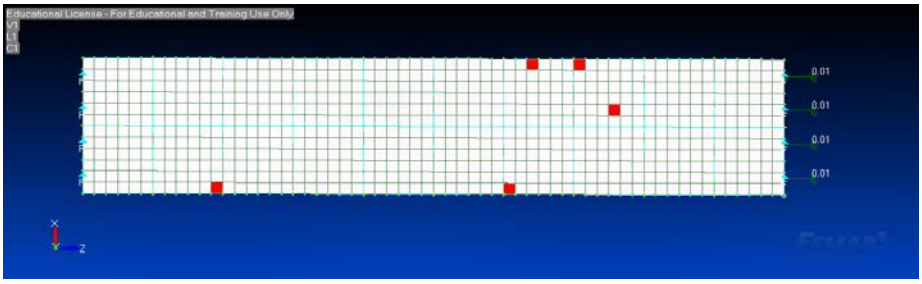

Figure 22. Element failure locations (shown in red) predicted during five analyses of a 1.02-mm-thick (0.04 in or 8 chips) tensile specimen

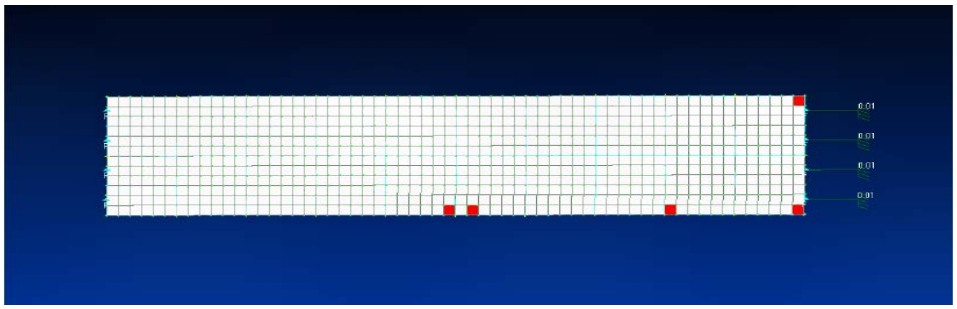

Figure 23. Element failure locations (shown in red) predicted during five analyses of a 2.30-mm-thick (0.09 in or 18 chips) tensile specimen

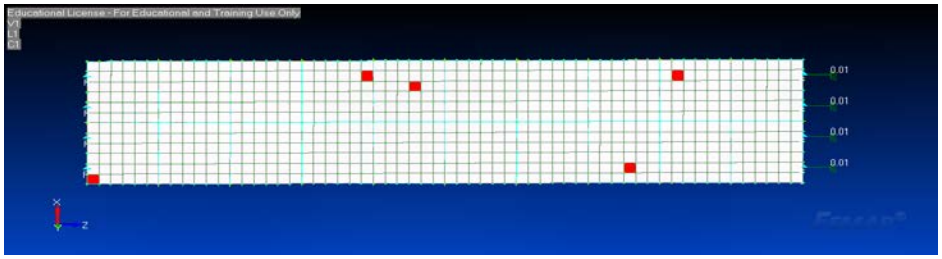

Figure 24. Element failure locations (shown in red) predicted during five analyses of a 4.06-mm-thick (0.16 in or 32 chips) tensile specimen

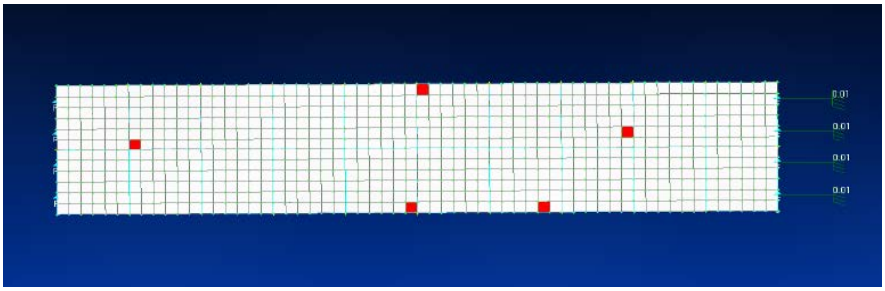

Figure 25. Element failure locations (shown in red) predicted during five analyses of a 5.80-mm-thick (0.23 in or 46 chips) tensile specimen

A comparison of figures 16 and 21 shows that predicted tensile stiffness and predicted tensile strength vary with thickness in a similar manner. That is, based on the analyses performed in this study, it is predicted that thin 1.02-mm (8-chip) HexMC tensile specimens will exhibit comparatively low stiffness and strength with high variability. Both stiffness and strength are predicted to increase as thickness is increased, reaching a nominally constant value at a thickness of approximately 3 mm (0.12 in = 24 chips). Variability is predicted to decrease with an increase in thickness. Note that the predicted tensile stiffnesses shown in figure 16 are based on 1500 analyses at each thickness, whereas the predicted tensile strengths shown in figure 21 are based on only five analyses at each thickness. Therefore, the trend in predicted tensile strengths shown in figure 21 should only be viewed as preliminary.

Stress-strain curves predicted for the four thicknesses considered are shown in figures 26–29. The slope of an individual curve generally decreases as stress is increased, reflecting the gradual reduction in overall specimen stiffness as distributed chip damage develops. Predicted average

and B-basis tensile strengths are presented in table 9 and plotted in the form of a bar chart in figure 30. Once again, note that these strength values are based on only five simulations. If a greater number of strength simulations had been performed, then the difference between average and B-basis strengths would likely have decreased. A greater number of strength simulations could not be completed during this study due to time and budget constraints.

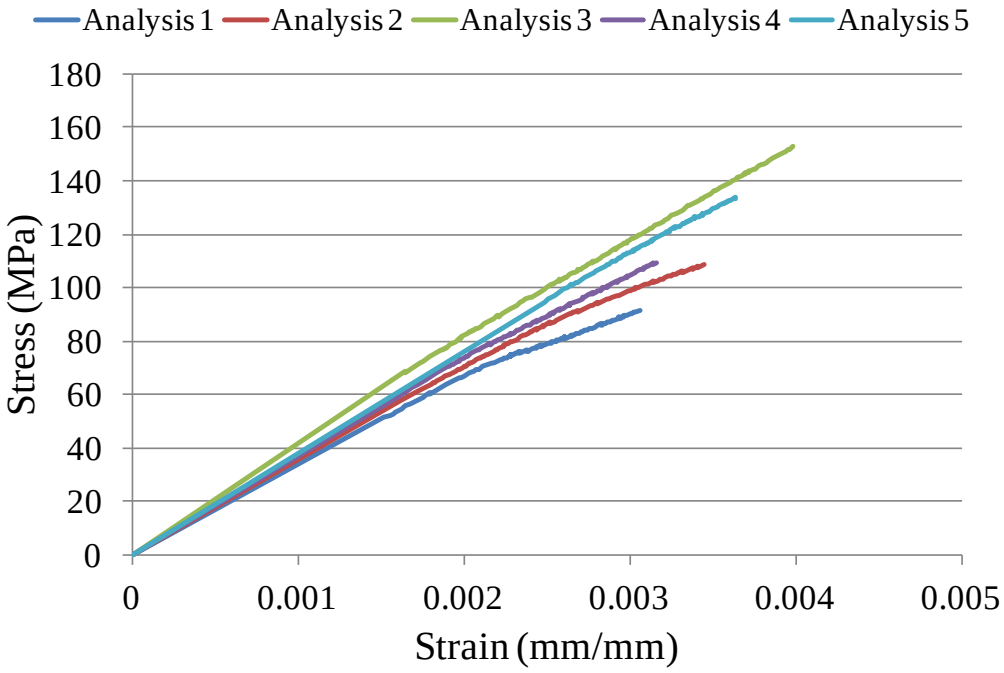

Figure 26. Stress-strain curves to fracture for unnotched thickness of 1.02 mm (0.04 in or 8 chips), based on criterion 1

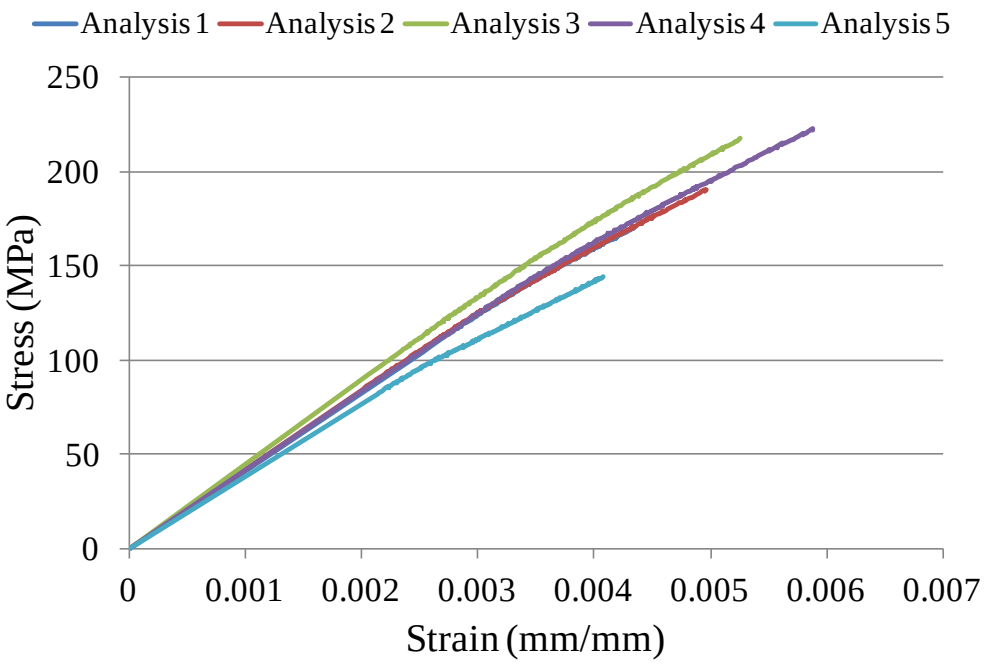

Figure 27. Stress-strain curves to fracture for unnotched thickness of 2.30 mm (0.09 in or 18 chips), based on criterion 1

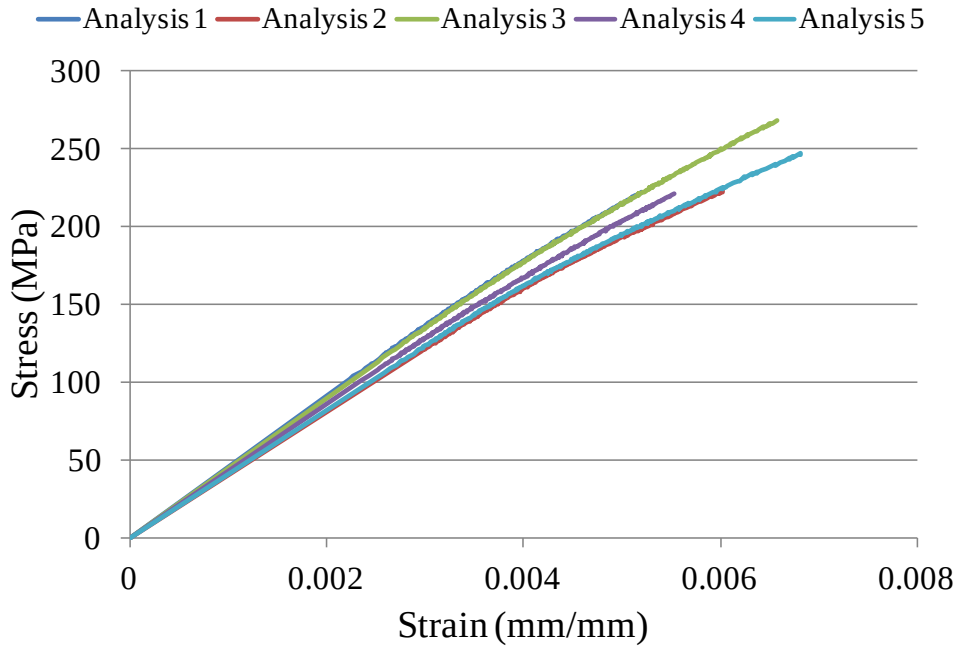

Figure 28. Stress-strain curves to fracture for unnotched thickness of 4.06 mm (0.16 in or 32 chips), based on criterion 1

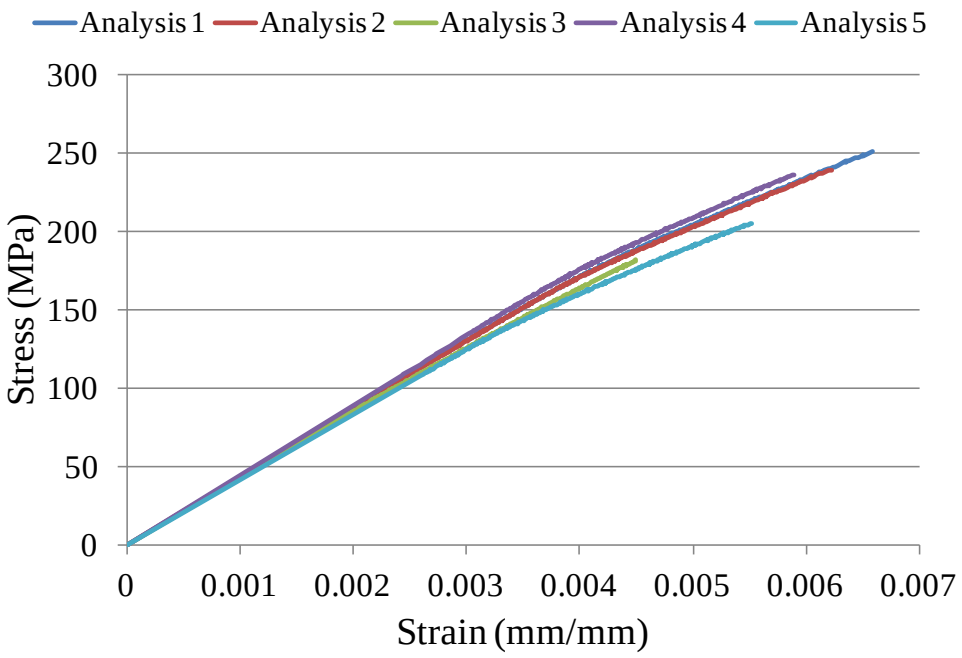

Figure 29. Stress-strain curves for fracture for unnotched thickness of 5.80 mm (0.23 in or 46 chips), based on criterion 1

Table 9. Average and B-basis fracture strengths for unnotched tensile specimens

Specimen Thickness	Average Strength	B-basis Strength
1.02 mm (0.04 in or 8 chips)	119.31 MPa (17.30 ksi)	20.85 MPa (3.02 ksi)
2.29 mm (0.09 in or 18 chips)	188.81 MPa (27.39 ksi)	54.56 MPa (7.91 ksi)
4.06 mm (0.16 in or 32 chips)	235.98 MPa (34.23 ksi)	149.78 MPa (21.72 ksi)
5.80 in (0.23 in or 46 chips)	222.74 MPa (32.31 ksi)	105.37 MPa (15.28 ksi)

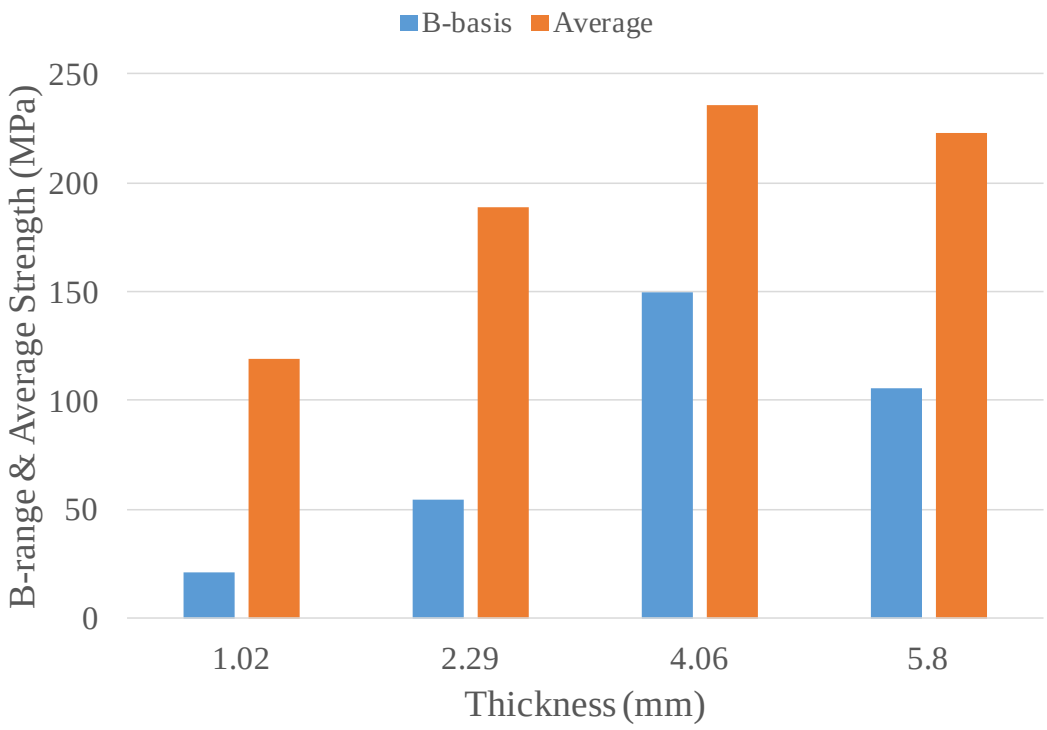

Figure 30. Predicted average and B-basis strength values for unnotched specimens

Five different fracture criteria were considered for use during this study. All fracture predictions presented thus far have been based on criterion 1, the computationally least expensive approach. Two fracture predictions were completed for 2.29-mm-thick (0.09 in or 18 chips) specimens based on criterion 4, the computationally most expensive approach. In these cases, fracture was declared when all chips in the model were predicted to have failed, rather than all the chips in a single element. Two predicted stress-strain curves based on criterion 4 are shown in figure 31. These analyses required approximately 30 hours (each) to complete. The fracture strength predicted during analyses 1 and 2 were 916 MPa and 775 MPa, respectively.

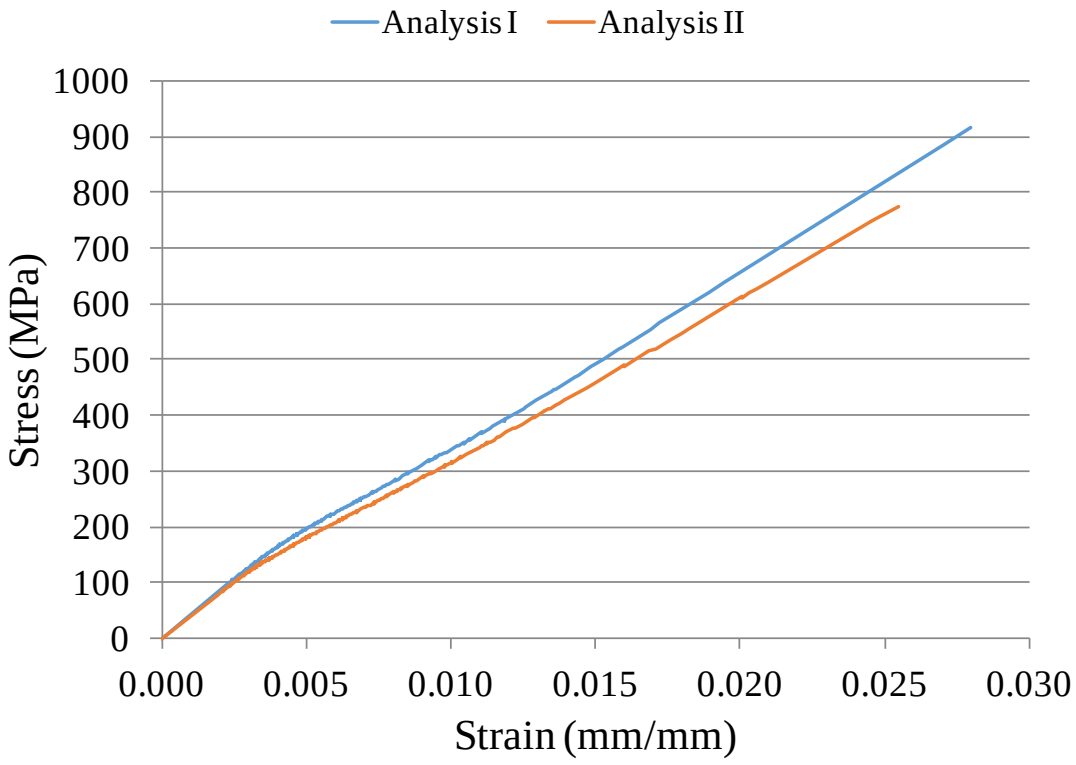

Figure 31. Stress-strain curves to fracture for unnotched thickness of 2.30 mm (0.09 in or 18 chips), based on criterion 4

Comparing these values to those presented in figure 27 and table 8, it is seen that the predicted fracture strength based on criterion 4 are approximately five times higher than those based on criterion 1.

It is obviously important to compare predicted and measured fracture strengths. However, it is also important to note that during this study (a) only five failure analyses per thickness were completed based on fracture criterion 1 (as summarized in figure 21), and (b) only two analyses for a single thickness were completed based on criterion 4 (figure 31). As previously explained the number of failure analyses was restricted during this study due to extensive computation times.

Because of the limited number of predicted strengths it is premature to compare predicted and measured failure strengths in a quantitative manner. However, a qualitative comparison was made. A proprietary HexMC database generated by the Hexcel Corporation was made available to the authors during this study. The database included 18 strength measurements at four specimen thicknesses: 2.3 mm, 3.6 mm, 5.8 mm, and 9.4 mm. The mean and standard deviation of the Hexcel strength measurements, normalized to the mean strength measured for a 2.3 mm thick specimen, are compared to predictions in figure 32. Although predicted values are for a different range in thickness compared to measured values, the qualitative agreement is evident.

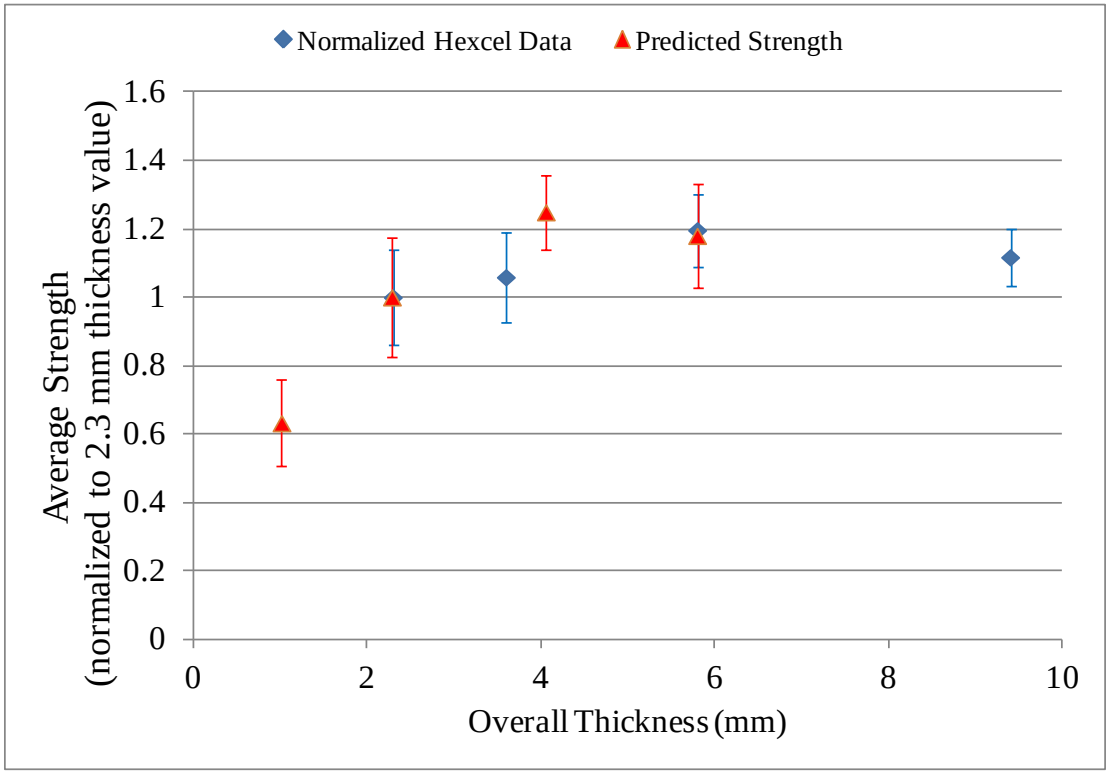

Figure 32. Comparision of predicted and measured normalized unnotched tensile strength (vertical lines represent normalized standard deviation)

4.2 OPEN-HOLE TENSILE STRENGTH

The SLA approach was used to predict open-hole tensile strengths of 2.3-mm-thick specimens (0.09 in or 18 chips) with a central circular hole of diameter *d*. Fracture was defined using criterion 1. Nominal specimen stress was calculated using the definitions of both gross stress and net stress:

$$\sigma^{gross} = \frac{P}{wt} \tag{12}$$

$$\sigma^{net} = \frac{P}{(w-d)t} \tag{13}$$

where P = load applied to specimen, w = specimen width, t = specimen thickness, and d = hole diameter.

A specimen width of 38.1 mm (1.5 in) was used. Strengths were predicted for three diameters: d = 3.18mm, 9.53 mm, and 12.7 mm (0.125 in, 0.375 in, and 0.500 in). The hole diameter to specimen width ratio (d/w) therefore ranged from 0.083–0.33. The finite-element meshes used in each case are presented in figures 33–35. Five simulations were completed for each hole diameter.

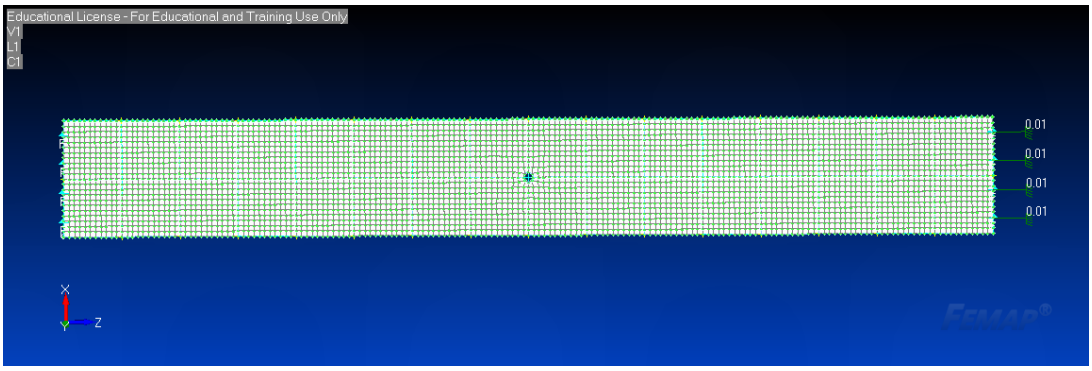

Figure 33. Mesh of notched specimen with a hole diameter of 3.18 mm (0.125 in)

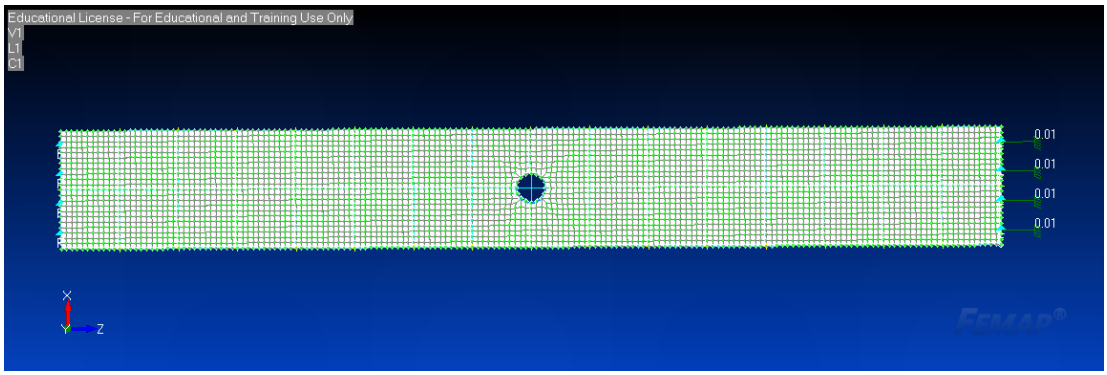

Figure 34. Mesh of notched specimen with a hole diameter of 9.53 mm (0.375 in)

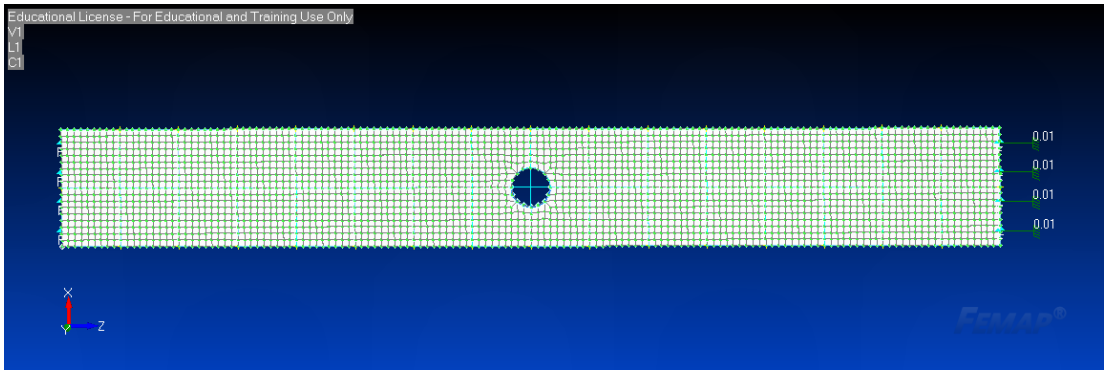

Figure 35. Mesh of notched specimen with a hole diameter of 12.7 mm (0.500 in)

Results of the analyses are summarized in tables 10–12. Figures 36–38 show plots of gross stress versus nominal axial strains for different notch diameters, whereas figures 39–41 show the location of the failed element predicted during each analysis. In this report, failures predicted to occur far from the hole are called gross section fractures, whereas those located at or near the hole are called net section fractures.

Table 10. Predicted strength results for *d/w* = 0.083 (hole diameter = 3.175 mm = 0.125 in)

Notch Diameter	Analysis Number	Gross Stress at Fracture	Net Stress at Fracture	Computation Time (hours)	Number of Failed chips	Type of Fracture
3.175 mm (0.125 in)	1	125.85 MPa (18.26 ksi)	137.29 MPa (19.91 ksi)	21	2,000	gross
	2	162.72 MPa (23.60 ksi)	177.51 MPa (25.75 ksi)	28	2,021	gross
	3	136.28 MPa (19.77 ksi)	148.67 MPa (21.57 ksi)	28	2,047	gross
	4	167 MPa (24.24 ksi)	182.3 MPa (26.44 ksi)	95	14,687	gross
	5	148.76 MPa (21.58 ksi)	160.40 MPa (23.26 ksi)	32	2,050	gross

Table 11. Predicted strength results for *d/w* = 0.25 (hole diameter = 9.52 mm = 0.375 in)

Notch Diameter	Analysis Number	Gross Stress at Fracture	Net Stress at Fracture	Computation Time (hours)	Number of Failed chips	Type of Fracture
9.53 mm (0.375 in)	1	114.35 MPa (16.59 ksi)	152.47 MPa (22.12 ksi)	13.15	2239	net
	2	139.60 MPa (20.25 ksi)	186.17 MPa (27.00 ksi)	25.13	3633	net
	3	133.12 MPa (19.31 ksi)	176.33 MPa (25.75 ksi)	34.88	5579	gross
	4	139.05 MPa (20.17 ksi)	185.40 MPa (26.89 ksi)	54.76	8796	gross
	5	137.78 MPa (19.99 ksi)	183.71 MPa (26.65 ksi)	22.98	3590	net

Table 12. Predicted strength results for *d/w* = 0.33 (hole diameter = 12.7 mm = 0.500 in)

Notch Diameter	Analysis Number	Gross Stress at Fracture	Net Stress at Fracture	Computation Time (hours)	Number of Failed chips	Type of Fracture
12.7 mm (0.50 in)	1	94.72 MPa (13.74 ksi)	142.07 MPa (20.61 ksi)	4.24	646	net
	2	124.18 MPa (18.01 ksi)	186.27 MPa (27.02 ksi)	8.92	1,733	gross
	3	115.96 MPa (16.82 ksi)	173.94 MPa (25.23 ksi)	4.52	838	net
	4	123.13 MPa (17.86 ksi)	184.70 MPa (26.79 ksi)	8.81	1,672	gross
	5	156.41 MPa (22.69 ksi)	104.27 MPa (15.13 ksi)	4.20	812	net

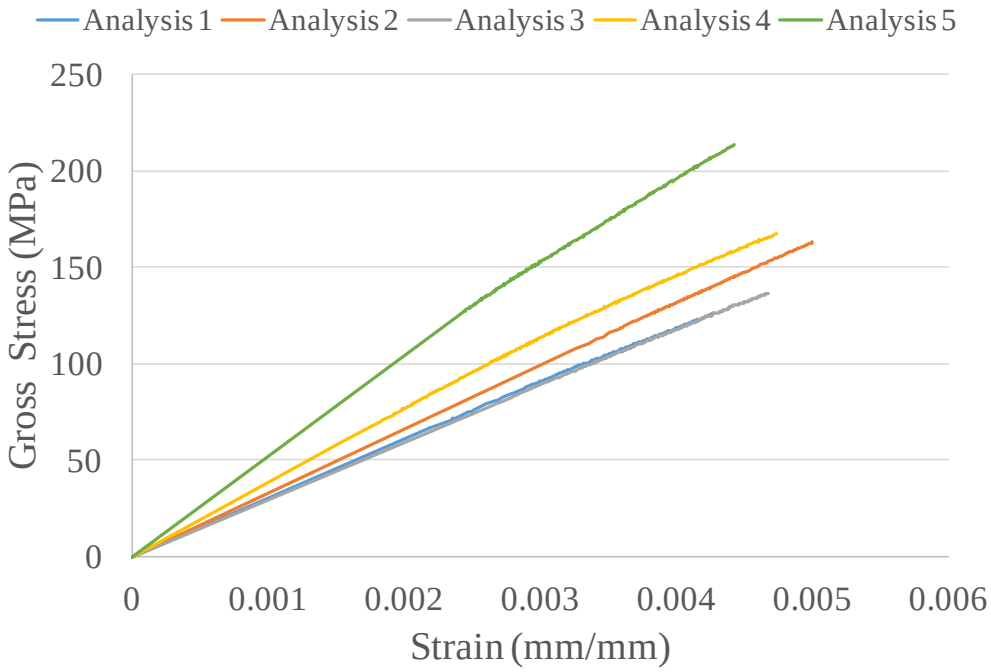

Figure 36. Predicted gross stress-strain curves for a hole diameter of 3.175 mm (0.125 in)

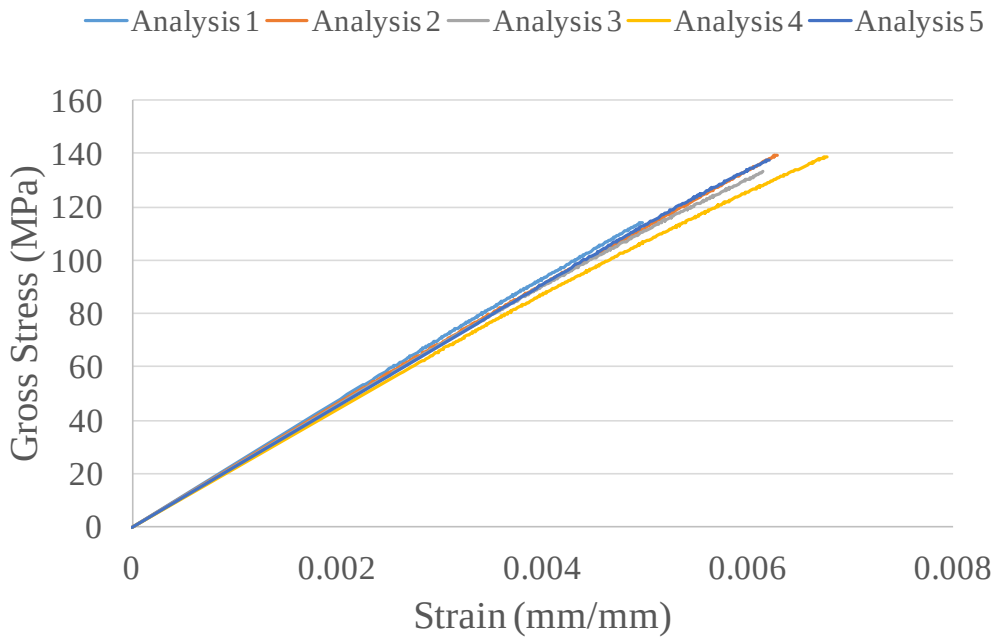

Figure 37. Predicted gross stress-strain curves for a hole diameter of 9.53 mm (0.375 in)

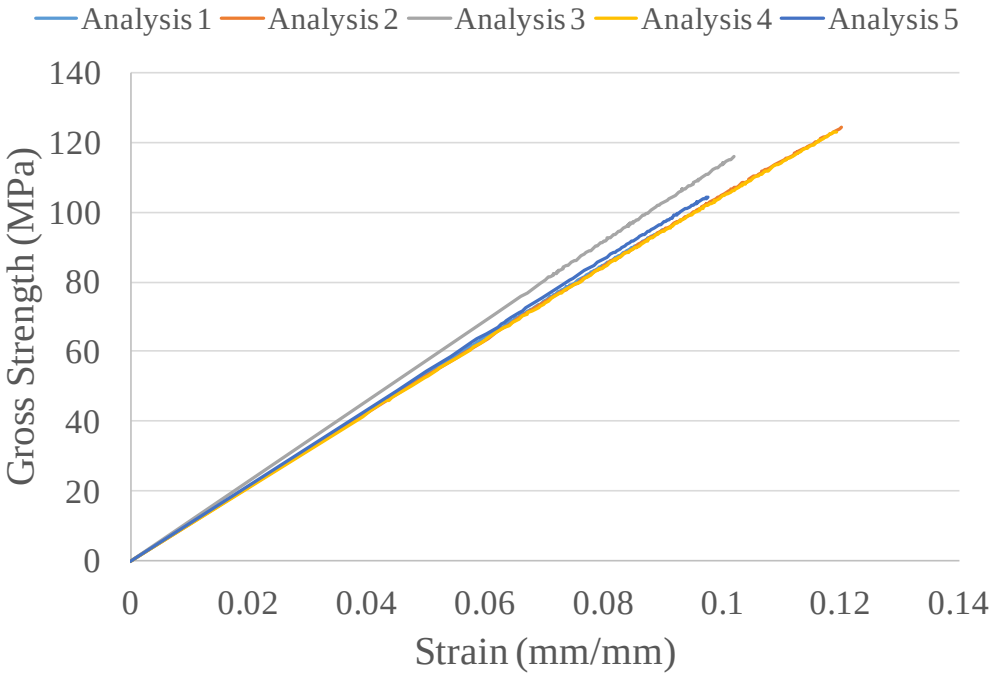

Figure 38. Predicted gross stress-strain curves for a hole diameter of 12.7 mm (0.50 in)

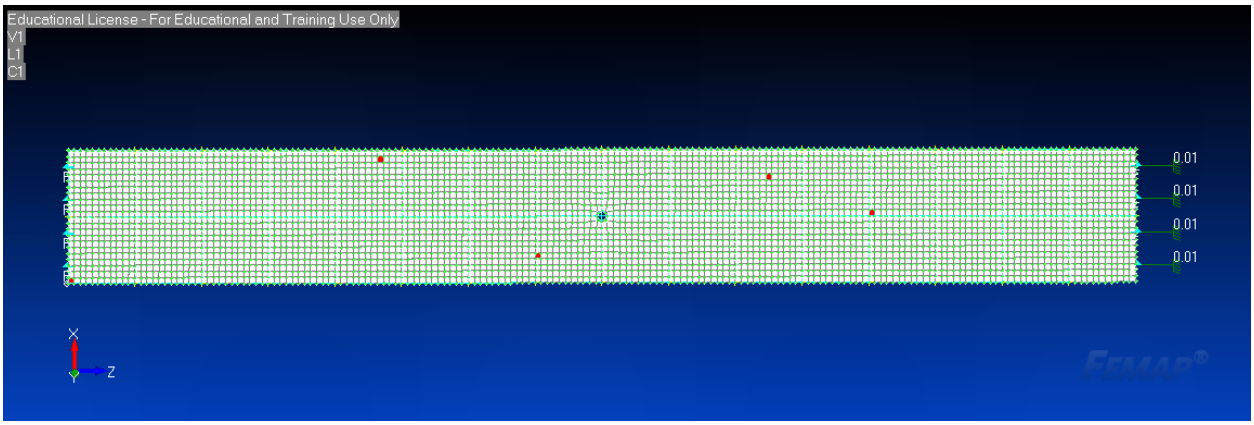

Figure 39. Predicted location of failed elements during five failure analyses based on a hole diameter of 3.175 mm (0.125 in)

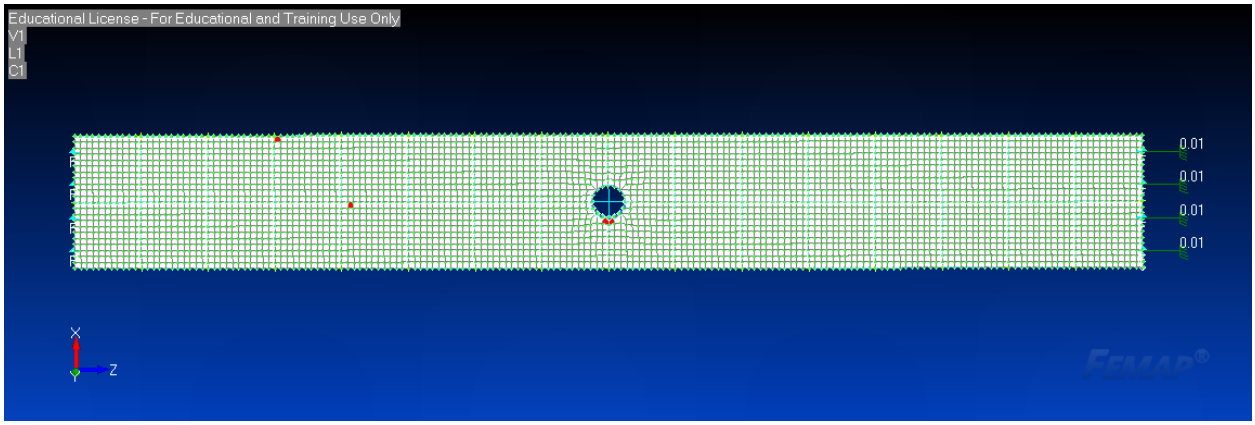

Figure 40. Predicted location of failed elements during five failure analyses based on a hole diameter of 9.53 mm (0.375 in)

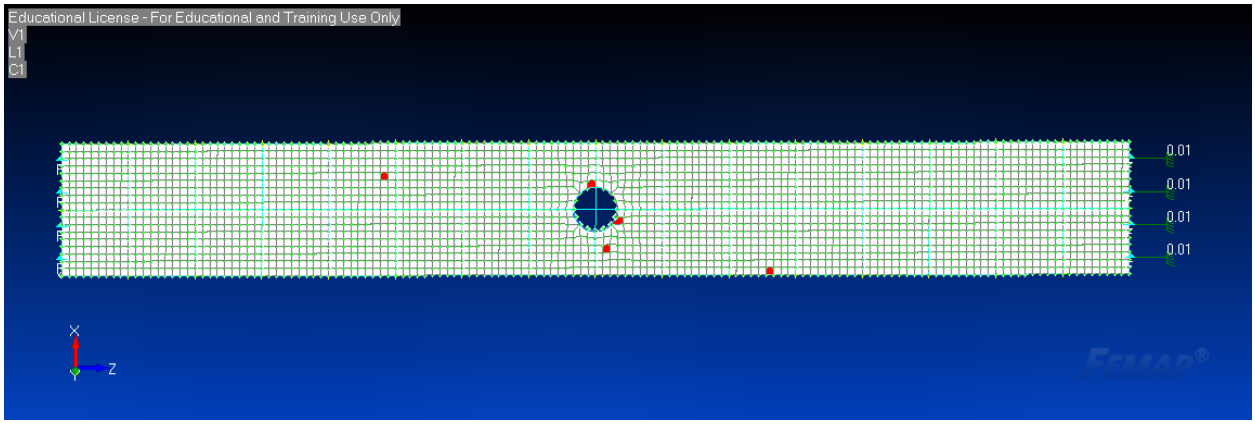

Figure 41. Predicted location of failed elements during five failure analyses based on a hole diameter of 12.7 mm (0.5 in)

Based on figures 39–41, it is concluded that HexMC open-hole tension specimens generally exhibit gross section failures for $d/w = 0.083$; however, net section fractures began to occur as the d/w ratio is increased. Specifically, five simulations were performed for $d/w = 0.083$ (hole diameter = 3.18 mm = 0.125 in), and gross section fractures were predicted in all five cases. In contrast, five simulations were completed for $d/w = 0.25$ and 0.33, and in both of these cases, net section fractures were predicted in three out of five simulations. This is in qualitative agreement with the experimental study of Feraboli et. al [7], who measured strictly gross section fractures for $d/w = 0.083$, but observed increasing occurrences of net section fractures as d/w is increased.

Predicted average and B-basis gross strengths are summarized in table 13 and plotted in the form of a bar chart in figure 42. Keep in mind that these predicted values are based on only five simulations for each hole diameter. It is likely that the difference between average and B-basis strengths would be reduced if a greater number of simulations had been completed. Still, the expected trend is predicted in the sense that that gross fracture stress is predicted to decrease as the d/w ratio is increased.

Table 13. Predicted average and B-basis open-hole tensile gross strengths

Notch Diameter	Average	B-basis
3.175 mm (0.125 in)	148.12 MPa (21.48 ksi)	76.85 MPa (11.15 ksi)
9.53 mm (0.375 in)	132.78 MPa (19.26 ksi)	89.22 MPa (12.94 ksi)
12.7 mm (0.50 in)	112.45 MPa (16.31 ksi)	60.33 MPa (8.75 ksi)

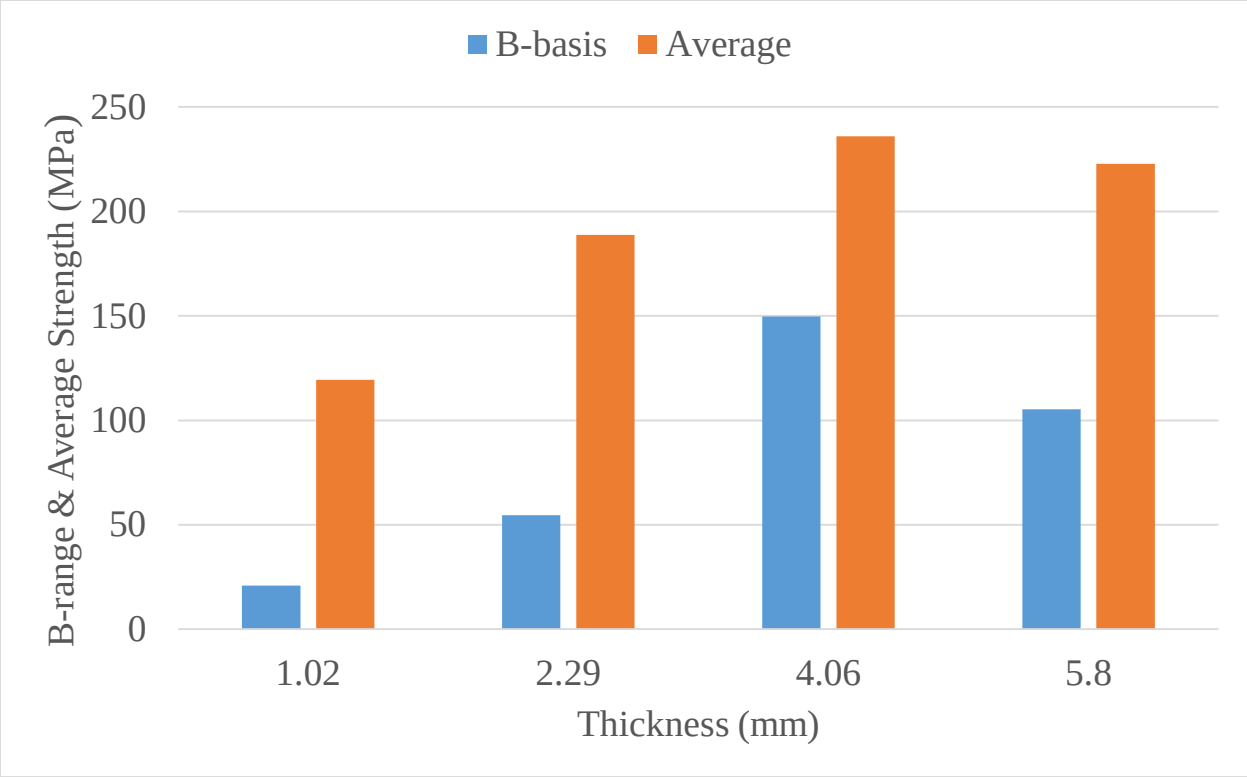

Figure 42. Predicted B-basis, average, and Bmax open-hole tensile gross strengths

5. SUMMARY AND CONCLUSIONS

The overall goal of this study was to assess a numerical modeling approach that will ultimately lead to a cost-effective certification process for discontinuous fiber composite (DFC) structures based on analysis and supported by modest experimental verification. A commercially available DFC material system known as HexMC™ was used as a model DFC during the study. The stochastic laminate analogy (SLA), a stochastic (Monte Carlo-type) finite element modeling approach, was developed and used to predict the stiffness and strength of HexMC tensile specimens. During a typical analysis, the HexMC specimen is divided into regions called random laminate volume elements (RLVEs). A unique randomly generated and non-symmetric stacking sequence is assigned to each RLVE. Stacking sequences in neighboring RLVEs are therefore completely independent. Experimentally observed variations in the tensile stiffness and notched and unnotched fracture strength of HexMC are then simulated by performing many finite-element analyses, in which a new random stacking sequence is generated for all RLVEs during each analysis. Fracture predictions were obtained through a damage accumulation model based on the ply discount scheme. A typical analysis predicts that ply failures (i.e., damage) evolve in a distributed manner throughout the HexMC specimen, even in the presence of stress risers. This damage pattern is in qualitative agreement with experimental observation. In this study, the SLA modeling approach was used to predict average, B-basis, and Bmax tensile stiffness and average and B-basis tensile strength.

It is predicted that relatively thin HexMC specimens (e.g., less than approximately 16–18 chips thick) will exhibit comparatively low average tensile stiffness with a high level of variation. As thickness is increased (for thicknesses of more than approximately 18 chips), average tensile thickness converges to a near-constant value, and the coefficient of value (CoV) decreases. The average tensile stiffness of thick HexMC specimens is predicted to be approximately 92% of the corresponding quasi-isotropic value, with a CoV of approximately 18%.

Fracture predictions were hampered by the extreme computational expense associated with the SLA approach. In addition, failure predictions were based on a failure criterion (the Tsai-Wu criterion) that cannot capture important failure modes, most notably delamination failures between chips. Nevertheless, the SLA approach was able to predict important experimental observations. For example, the analysis showed that fractures of open-hole tensile specimens with a *d/w* ratio of less than approximately 0.083 will normally occur away from the hole, rather than at the hole. As the hole size is increased (i.e., as the *d/w* ratio is increased), the likelihood of fracture at the hole is increased. Most fractures will occur at the hole for *d/w* greater than 0.33.

Though further development is required, the SLA approach shows great promise in predicting the elastic and fracture behavior of DFC structures. Once perfected, the SLA approach may lead to an enormous decrease in certification costs of DFC aircraft structures. The primary areas of improvement needed are an improved chip failure model (used to predict the evolution of distributed damage and final fracture) and a substantial reduction in computation times. During this study, the analysis involved the use of four separate software programs/packages: a Visual Basic program (written in-house), Femap, NX Nastran, and Excel. In future studies a substantial reduction in computation times might be achieved by simply consolidating these four software programs/packages into a single process. If consolidation does not result in a sufficient reduction in computation times then a further reduction can be achieved through the use of a high-speed computer cluster.

6. REFERENCES

1. N.A. (2006). Boeing 787: From the ground up. *Aero*, 4.06. Retrieved from http://www.boeing.com/commercial/aeromagazine/articles/qtr_4_06/article_04_2.html.

2. A350 XWB: The Xtra that makes the difference. Retrieved from http://www.airbus.com/aircraftfamilies/passengeraircraft/a350xwbfamily/technology-and-innovation/.

3. Custom formulated sheet & bulk molding compounds. *IDI Composites International: Ideas for Meaningful Results.* Retrieved from http://www.idicomposites.com/smc-bmc-overview.php.

4. Hexel Corporation. (2011, September). As Boeing delivers the first 787 Dreamliner, Hexcel reveals some of their composite innovations for the aircraft. *Hexcel.* Retrieved from http://www.hexcel.com/news/market-news/news-20110926.

5. Hexel Corporation. (2008, May). Hexcel to supply carbon fiber composites for Airbus A350 XWB primary structures. *Hexcel.* Retrieved from http://www.hexcel.com/news /archive/news-20080530.

6. Feraboli, P., Peitso, E., Cleveland, T., & Stickler, P. B. (2009). Modulus measurement for prepreg-based discontinuous carbon fiber/epoxy systems. *Journal of Composite Materials. 43*(19), 1947-1965, DOI: 10.1177/0021998309343028.

7. Feraboli, P., Peitso, E., Cleveland, T., & Stickler, P. B. (2009). Notched behavior of prepreg-based discontinuous carbon fiber/epoxy systems, *Composites: Part A Applied Science and Manufacturing, 40*(3), 289–299, DOI:10.1016/j.compositesa.2008.12.012.

8. Head, B. H. (2013). *Analysis methods for discontinuous fiber composites* (Master's thesis). Retrieved from https://digital.lib.washington.edu/researchworks/bitstream/handle /1773/24164/Head_washington_0250O_12097.pdf?sequence=1.

9. Arce, M. R. (2015). *Certification of discontinuous composite material forms for aircraft structures.* (Master's thesis). Retrieved from https://digital.lib.washington.edu/ researchworks/bitstream/handle/1773/34044/Arce_washington_0250O_15178.pdf?seque nce=1.

10. Halpin, J. C., & Pagano, N. J. (1969). The laminate approximation for randomly oriented fibrous composites. *Journal of Composite Materials, 3*(4), 720–724, DOI: 10.1177/002199836900300416.

11. Halpin, J. C, & Kardos, J. L. (1978). Strength of discontinuous reinforced composites: I. Fiber reinforced composites. *Polymer Engineering and Science, 18*(6), 496–504, DOI: 10.1002/pen.760180612

12. Halpin, J. C., Jebine, K., & Whitney, J. M. (1971). The laminate analogy for 2 and 3 dimensional composite materials. *Journal of Composite Materials, 5*(1), 36–49, DOI: 10.1177/002199837100500104.

13. Feraboli, P., Cleveland, T., Stickler, P., & Halpin, J. (2010). Stochastic laminate analogy for simulating the variability in modulus of discontinuous composite materials. *Composites: Part A. Applied Science and Manufacturing,* 41(4), DOI:10.1016/j.compositesa.2010.01.003.

14. Head, B. H. & Tuttle, M. E. (2013). *Certification of discontinuous composite material forms of aircraft structures.* Paper presented at JAMS 2013 Technical Review, Wichita, KS.

15. Hexcel. (n.d.). HexMC materials for industries. Retrieved from http://www.hexcel.com/ products/industries/ihexmc-materials.

16. Marlett, K. (2011, May). Hexcel 8552 AS4 unidirectional materials property data report. Retrieved from http://www.niar.wichita.edu/coe/ncamphexcel.asp.

17. McGowan, D. M., & Ambur, D. R. (1998, January). *Damage characteristics and residual strength of composite sandwich panels impacted with and without compression loading.* Paper presented at the 39th AIAA/ASME/ASCE/AHS/ASC SSDMC Conference, Long Beach, CA.

18. FAA Report. (2003). *Material Qualification and Equivalency for Polymer Matrix Composite Material Systems: Updated Procedure* (DOT/FAA/AR-03/19).

19. Shyprykevich, P. (1989, January). The role of statistical data reduction in the development of design allowables for composites. In C. C. Chamis (ed.), *Test methods for design allowables for fibrous composites: 2nd volume*. Paper presented at the meeting of the American Society for Testing and Materials, Philadelphia, PA.

20. Tuttle, M. E. (2013). Structural analysis of polymeric composite materials, 2nd edition. Boca Raton, FL: CRC Press, Taylor & Francis Group.

21. N.A. (2004, October). *Moving closer to the goal of cost-effecive complex geometry carbon composite parts*. Paper presented at the 19th Joint American Society For Composites / American Society For Testing And Materials Committee D30 Technical Conference, Atlanta, GA.